Water vapour self-continuum in near-visible IR absorption bands: measurements and semiempirical model of water dimer absorption

Water vapour self-continuum in near-visible IR absorption bands: Measurements and semiempirical model of water dimer absorption

Anna A. Simonova[a], Igor V. Ptashnik[a], Jonathan Elsey[b], Robert A. McPheat[c], Keith P. Shine[b], Kevin M. Smith[c]

[a] Atmospheric Spectroscopy Division, V.E. Zuev Institute of Atmospheric Optics, Siberian Branch of the Russian Academy of Sciences, Tomsk, 1 Academician Zuev square, 634055, Russia
[b] Department of Meteorology, University of Reading, Reading, RG66BB, UK
[c] Rutherford Appleton Laboratory, Didcot, Oxfordshire, OX11 0QX, UK

Corresponding author: Igor V. Ptashnik (piv@iao.ru)

Abstract

The nature of the water vapour continuum has been of great scientific interest for more than 60 years. Here, water vapour self-continuum absorption spectra are retrieved at temperatures of 398 K and 431 K and at vapour pressures from 1000 to 4155 mbar in the 8800 and 10600 cm^{-1} absorption bands using high-resolution FTS measurements. For the observed conditions, the MT_CKD-3.2 model underestimates the observed continuum on average by 1.5–2 times. We use the hypothesis that water dimers contribute to the continuum absorption to simulate the experimentally-retrieved self-continuum absorption spectra, and to explain their characteristic temperature dependence and spectral behaviour. The values of the effective equilibrium constant are derived for the observed temperatures. We find that the dimer-based model fits well to the measured self-continuum from this and previous studies, but requires a higher effective equilibrium constant compared to the modern estimates within the temperature range (268-431 K) and spectral region studied. It is shown that water dimers are likely responsible for up to 50% of the observed continuum within these bands. Possible causes of the incomplete explanation of the continuum are discussed. Extrapolating these measurements to atmospheric temperatures using the dimer-based model, we find that the newly-derived self-continuum reduces calculated surface irradiances by 0.016 W m^{-2} more than the MT_CKD-3.2 self-continuum in the 8800 cm^{-1} band for overhead-Sun mid-latitude summer conditions, corresponding to a 12.5% enhancement of the self-continuum radiative effect. The change integrated across the 10600 cm^{-1} band is about 1%, but with significant differences spectrally.

Keywords: continuum absorption, water vapor, absorption band, water dimer, line wings, semiempirical model

1. Introduction

As one of the main gaseous absorbers of solar radiation, water vapour plays an important role in radiative processes occurring in the Earth's atmosphere. Positive feedback between water vapour concentration and temperature of the Earth's surface significantly affects the weather and climate of the Earth. Part of the water vapour absorption, the so-called water vapour *continuum*, has been a special subject of study since it was first measured in the mid-infrared atmospheric window (8–14 μm) in 1918 [1]. Whilst we have a good understanding of the mechanisms responsible for water vapour absorption lines, the physics underlying the water vapour continuum is not yet as clear. The

intensity of the latter is characterized by a slowly varying spectral dependence that makes a small contribution to the total absorption of solar radiation by water vapour in the Earth's atmosphere (up to 3% in the global average) [2]. The spectrum of water vapour continuum absorption can be divided into so-called *self* and *foreign* components. The former is a result of interactions between water molecules, while the latter is caused by the interaction of water molecules with other gases, most notably nitrogen and oxygen in the Earth's atmosphere. This paper focuses on improved understanding of the water vapour *self-continuum*. Despite the much stronger intensity of water absorption lines compared to the underlying continuum, there are particular features of the latter that allow it to be spectrally discerned. A strong negative exponential temperature dependence and quadratic pressure dependence of the water vapour self-continuum absorption are among such features.

From an atmospheric radiative transfer perspective, the most relevant contributions of the self-continuum absorption to the water vapour absorption spectrum are located predominantly in the atmospheric window regions, where the spectral lines are relatively weak. In these atmospheric windows, there is significant interest in the continuum absorption for several applications. For example, the continuum strongly impacts the radiative balance of the atmosphere, affects the propagation of laser radiation through the atmosphere and can interfere with the retrieval of atmospheric gases, aerosols and clouds by optical methods [3].

Depending on the spectral region, the continuum within water absorption bands is between two and three orders of magnitude weaker than the overlying spectral lines. Nevertheless, even within these bands, the continuum absorption can be comparable with the local line absorption or even dominate it in many microwindows between spectral lines, which makes it distinguishable in measurements with sufficient spectral resolution. The first laboratory identification of water dimer spectral features in the in-band near-IR self-continuum was presented in [4,5] using the calculated dimer spectrum from [6]. Since then, distinct spectral peaks have been discovered in the measurements of the continuum absorption spectrum within other near-IR water vapour bands [4,7–9], which have allowed conclusions to be drawn about the nature of this component of the continuum. Therefore, the investigation of the continuum absorption within the bands has significance for our fundamental understanding of the underlying physics.

There are two physical mechanisms that are most often cited as being responsible for the continuum absorption in the IR and mm-wave spectral regions, both of which likely contribute to a certain extent in different spectral regions: (a) the cumulative absorption of the far wings of strong water monomer spectral lines [10–15], and (b) bound and quasibound water dimers[1] (b- and q-dimers, respectively) [7–9,16–21]. The first of these mechanisms, far-wing absorption, results from energetic collisions between water molecules, which perturb rovibrational energy levels. There are two main approaches to the far-wing hypothesis: asymptotic [12,15] and quasistatic [13,14]. Both approaches operate in terms of intermolecular potential and use a set of parameters derived by fitting models to experimental data. A satisfactory agreement of the far-wing model with the experimental continuum has been shown [22,23] in some atmospheric windows in the far and middle IR spectral regions. However, the existing far-wing models cannot provide sufficient accuracy in predicting the intensity or temperature dependence of the continuum absorption over a wide spectral region without

[1]Bound (or stable) dimers require a third-body collision for their formation; quasibound (or metastable) dimers relate to multiple-approach pair collisions resulting in the temporary stabilization of a pair which has total internal energy in excess of the dissociation threshold.

a number of experimentally fitted *ad hoc* parameters that cannot be verified from independent sources.

The second mechanism, which is based on water dimer absorption, describes the main temperature and spectral dependences of the continuum absorption well (see, for instance, [24]) after adjusting just two physically-based parameters (the dimer equilibrium constants) to fit the experimental data. Bound and quasibound dimers exhibit different properties (e.g. dissociation energy and lifetime), and consequently they are expected to have different spectral features. Moreover, a statistical approach shows that absorption from either of these states can be the dominant contributor tocontinuum absorption depending on the thermodynamic conditions [19]; b-dimers dominate at lower temperatures and q-dimers are more prevalent at higher temperatures. The 'transition' temperature depends on the intermolecular potential and is different for different molecular pairs. For example, for water dimers the transition temperature is expected to be close to room temperature [19].

The absorption by water dimers is a dominant mechanism of so-called bimolecular absorption by water vapour (see, for instance, [19]) at near atmospheric conditions. With increasing temperature, the contribution of the third form of bimolecular absorption–free H_2O pairs[2]–begins to increase: from negligible at room temperature to dominant at very high temperatures. Since this mechanism becomes noticeable only at temperatures much greater than the temperature range of 398-431 K investigated here, it is not considered further. Earlier considerations of the possible absorption of solar radiation by water dimers in the visible and near-IR regions were presented in [25,26] based on the first calculated water dimer vibrational spectra. To this day, quantum-chemical calculations of water dimer spectra are still challenging, especially at higher wavenumbers (in near-infrared and visible regions). Nevertheless, quantum-chemical and quantum-mechanical calculations [27–29] that are now available together with the experimental data in the microwave [30,31], mid-infrared [3,32] and near-infrared [4–8] spectral regions, demonstrate the explicit involvement of water dimers in the water vapour continuum spectrum.

For practical applications, the MT_CKD continuum model is commonly used [33]. It is a semiempirical model, which modifies the Lorentzian profile in the line wings using a special χ-function, assuming a so-called "weak interaction" between molecules, which is more important for the in-band continuum, and makes a number of other empirical adjustments to fit the model to experimental data. The model has therefore changed significantly since it was described in [33] as new observations have become available; however many of these changes are not yet described in the literature. In the spectral regions analysed here the MT_CKD continuum has not been subjected to any experimental constraints and needs to be evaluated using observations. Although MT_CKD is primarily intended for application at atmospheric temperatures, the form of its temperature dependence is based on extrapolation of laboratory measurements made between temperatures of 296 and 338 K [33] in bands at lower wavenumbers and hence it may not be appropriate in other bands or at other temperatures.

This paper focuses on the investigation of the water vapour self-continuum absorption at elevated temperatures (398 and 431 K) and pressures (1000-4155 mbar) in the near-visible absorption bands centred at 8800 and 10600 cm^{-1} (1.13 and 0.94 μm) using laboratory observations. To our knowledge these are the first reported measurements of the self-continuum in these bands. These

[2] Free pairs are two water monomers, which experience one-off collisions and influence each other weakly.

measurements are then interpreted in terms of the water dimer hypothesis. This work is an extension of earlier investigations [24] on the origin of the continuum in the 1600 and 3600 cm^{-1} (6.25 and 2.7 μm) absorption bands at close to room temperature. Finally, calculations of the atmospheric absorption due to this continuum are presented, by using a dimer-based model to extrapolate the measurements to atmospheric conditions.

The paper structure is the following. Section 2 contains the main details of the measurements. In Section 3, the measurement errors are considered. The retrieval procedure of the water vapour continuum is described in Section 4. The water dimer model of the continuum is presented in Section 5 and is discussed in Section 6. Section 7 contains the estimate of the effect of the newly-retrieved water vapour continuum to the atmospheric absorption. Conclusions are summarized in Section 8. The retrieved water vapour continuum data are given in the Appendix and in the Supplementary Materials 1 and 2.

2. Experiment

The pure water vapour absorption spectra were obtained at the Molecular Spectroscopy Facility, Rutherford Appleton Laboratory (UK) in the near-visible spectral region 8500–13000 cm^{-1}. The experimental setup included a Bruker IFS 125HR Fourier Transform spectrometer (FTS), multipass absorption cell with optical path lengths of 9.7 and 17.7 m, Si-diode detector, 50 W quartz tungsten halogen bulb and vacuum system. In order to detect the weak continuum absorption in these absorption bands, the measurements were carried out at elevated water vapour pressures up to 4155 mbar and temperatures of 398 and 431 K (see measurement details in Table 1). The relative humidity did not exceed 75% to avoid water vapour condensation on the cell walls; the mirrors were also checked visually for any evidence of condensation. The total optical path lengths in the multipass absorption cell were 9.7 m for pressures above 3000 mbar and 17.7 m for lower pressures. The spectral resolution varied from 0.1 to 0.4 cm^{-1} depending on pressure and was about 0.2−0.25 of an average halfwidth of a spectral line.

A set of absorption spectra of pure water vapour at various pressures and temperatures were obtained. Each measurement was conducted in three stages to reduce the error in determining the baseline: (1) a background absorption spectrum of pure argon at the same pressure as the water vapour pressure in step 2; (2) a sample absorption spectrum of pure water vapour; (3) repeat of stage 1. The background measurements with argon were found to be more effective than measurements of an empty cell. Argon does not absorb radiation in this spectral region and was therefore useful to minimise possible effects of cell deformation on optical alignment caused by the elevated gas pressures. The baseline spectrum was derived as an average of the two background spectra.

Table 1 Thermodynamic conditions and configuration of pure water vapour absorption spectra measurements

Temperature, K	Spectral interval, cm^{-1}	Pressure, mbar	Optical length, m	Resolution, cm^{-1}
398	8505–9200, 10135–11110	1000 (6% ↓) 1370 (8.7%↓)	17.7	0.1 0.2
431	8530–9195, 10055–11110	1080 (3% ↑) 1580 (3% ↑) 2070 (1.5% ↑) 2101 (1.3% ↑)	17.7	0.1 0.2 0.2 0.2
		3145 (2.4% ↑) 4155 (3% ↑)	9.7	0.4 0.4

* The pressures given here are the spectroscopically-adjusted values using the method described in Section 3.2. The arrows indicate the reduction (↓) or increase (↑) due to this adjustment.

The experimental optical depth of water vapour absorption $\tau(v, T)$ at wavenumber ν and temperature T was derived from the Beer–Lambert law. An example of an optical depth spectrum of water vapour in the spectral region investigated is shown in Fig.1.

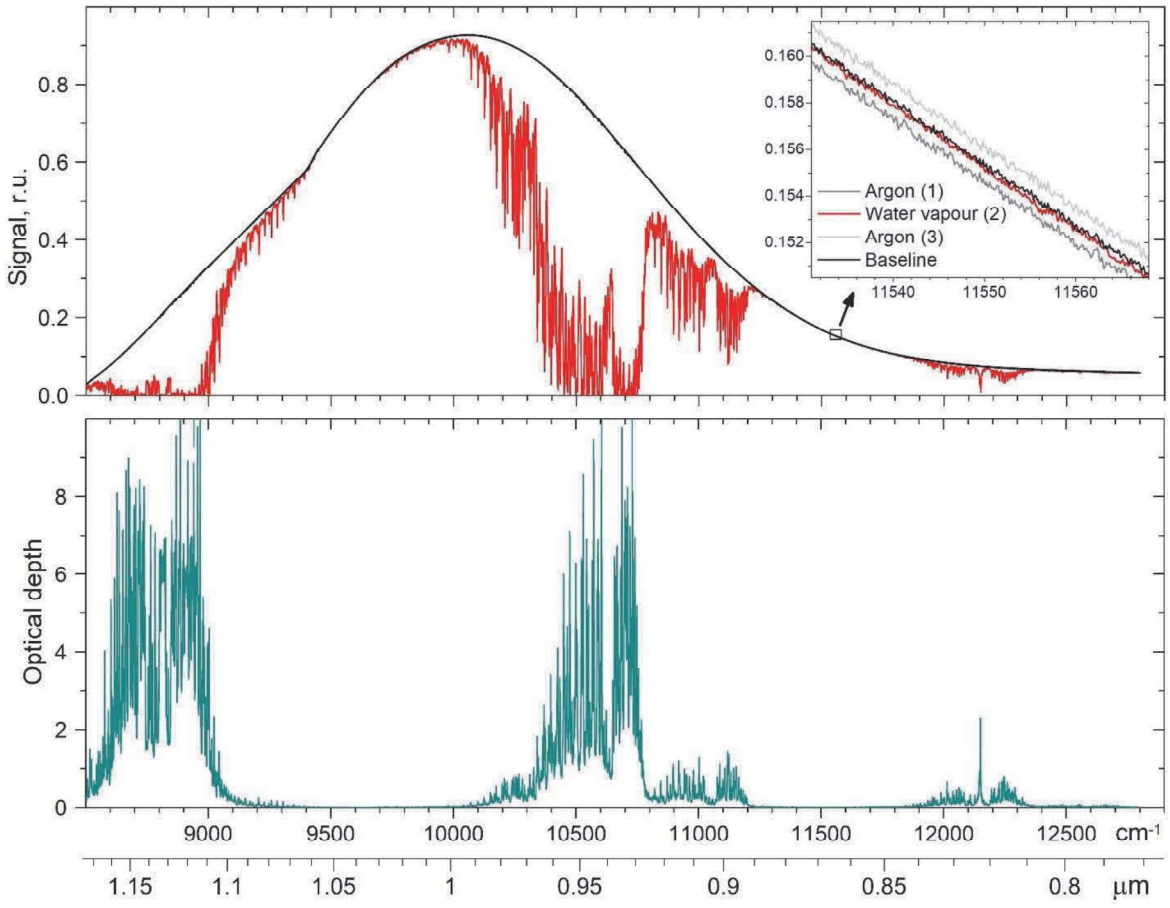

Fig. 1. FTS signals from measurements in the cell with argon (blackcurve) and water vapour (red curve) at a pressure of 3145 mbar and temperature of 431K (upper panel); the resulting spectrum of pure water vapour optical depth (dark cyan curve, bottom panel). To demonstrate the small baseline uncertainty, the insetin the upper panel shows the water vapour signal (red curve) and the baseline signal (blackcurve)obtained as an average of the signals from the cell with argon measured before (steps 1, light grey curve) and after (steps 3, dark grey curve) the sample measurements in a "window" spectral region where the continuum absorption is very weak compared to the in-band region. The kink in the baseline at about 9400 cm^{-1} is due to the detector's sensitivity function.

Deriving the water vapour continuum absorption from high-resolution absorption spectra first requires the calculation and subtraction of the local contribution from water monomer lines. These calculations were made using the LBL_{IAO} line-by-line program [34]. The local line contributions were calculated within 25 cm^{-1} from the centre of each Lorentzian line without the CKD "plinth". Water vapour line parameters were taken from HITRAN-2016 [35]. The continuum data beyond 11150 cm^{-1} demonstrate weak values compared to the noise level; therefore, only the 8800 and 10600 cm^{-1} absorption bands are investigated. The retrieval of the watervapour continuum at higher wavenumbers requires more sensitive measurements, for example, using the CRDS technique [36].

3. Error analysis

3.1 Error types

Discussionof the main sources of uncertainties for FTS measurements of the weak continuum absorption can be found, for example, in [37]. Here, four main error sources of error were identified and taken into account.

3.1.1 Random measurement error caused by the FTS system.

This error was evaluated by comparison of the noise within formation content at an optical depth of 1. To minimize this noise each measurement was averaged over hundreds of individual spectrometer scans. As a result, the information-to-noise ratio was not less than 500:1.

3.1.2 A quasi-random error due to uncertainties in spectral line parameters used for the water vapour spectra calculations.

Although these errors do not depend on time, they are often not correlated with each other and have a random character over the spectrum. Error codes given in the HITRAN database for the line centres, intensities, temperature coefficients, and pressure broadening coefficients were used to estimatethe upper limit of the absolute error of this type (see details in [38]).

3.1.3 Systematic errors caused by uncertainty in the spectral baseline (the FTS signal recorded when the cell contained argon).

The baseline was derived as an average of the signals obtained in measurements with argon before and after the water vapour absorption measurements. The inset in Figure 1 shows an example in a window spectral region around 11550 cm^{-1} where the continuum absorption should be negligible under the experimental conditions. These errors may be caused by slow temporal drifts in the spectrometer system or gas cell, and for individual measurements were partially mitigated by equal separation in time of background spectra acquisitions in relation to that of the water sample. However, this type of error is usually negligible for the measurements of in-band continuum absorption and does not exceed 1% in our case (see upper panel in Fig. 1).

3.1.4 Systematic errors caused by the inaccuracy in measured water vapour pressure and temperature.

The main uncertainty here was from the pressure measurements. A description of how these errors were reduced using a spectroscopic technique is given in Section 3.2.

3.2 Adjustment of the water vapour pressure

The measured intensities of water vapour absorption lines are proportional to the water vapour pressure, while the intensity of the continuum absorption is proportional to the square of the vapour pressure. Therefore, the precise value of the water vapour pressure plays an important role in retrieval of the water vapour continuum. To reduce the respective systematic error in this work, we performed a spectroscopic assessment of the measured water vapour pressures by comparing measured and calculated line intensities using the HITRAN database.

To exclude lines which are very weak or saturated, and lines with uncertain spectral parameters, we selected only spectral lines that have measured optical depths in the range 0.2 to 5 at line centre and an error-index for the line intensity and self-broadening of not less than 5 in HITRAN-2016. Then the measured intensities of the selected spectral lines were compared with

those calculated line-by-line using the HITRAN-2016 parameters within a distance of a few halfwidths from the line centre. Figure 2 shows an example of a distribution of relative deviation for each selected i-th line ($\delta I(\nu_i)$) in the investigated spectral region calculated using the equation:

$$\delta I(\nu_\mathrm{i}) = \frac{I_\mathrm{RAL}(\nu_\mathrm{i}) - I_\mathrm{HIT16}(\nu_\mathrm{i})}{I_\mathrm{RAL}(\nu_\mathrm{i})}. \qquad (1)$$

In Eq. (1), $I_\mathrm{RAL}(\nu_\mathrm{i})$ and $I_\mathrm{HIT16}(\nu_\mathrm{i})$ are line intensities obtained from the experiment and simulation, respectively. The average relative deviation between measured and calculated intensities of all selected lines was used as a criterion for the water vapour pressure adjustment factor. Systematic divergence of the $\delta I(\nu_\mathrm{i})$ distribution from zero indicates inaccuracy in the measured water vapour pressure. At the same time, strong deviations of $\delta I(\nu_\mathrm{i})$ were also observed for individual lines, which may be caused by errors in the parameters of relatively weak water vapour lines in the spectral database. Generally, the discrepancy was 4% on average in our measurements and we adjusted the pressures to agree with the spectroscopically-derived values (see Table 1).

Measurements at T=471 K were also performed in this work. However, at some pressures these measurements had poor agreement between the measured and spectroscopically-derived pressure, as well as poor agreement with the pressure-squared dependence expected for the self-continuum absorption. Therefore, we excluded these measurements from analysis in this paper.

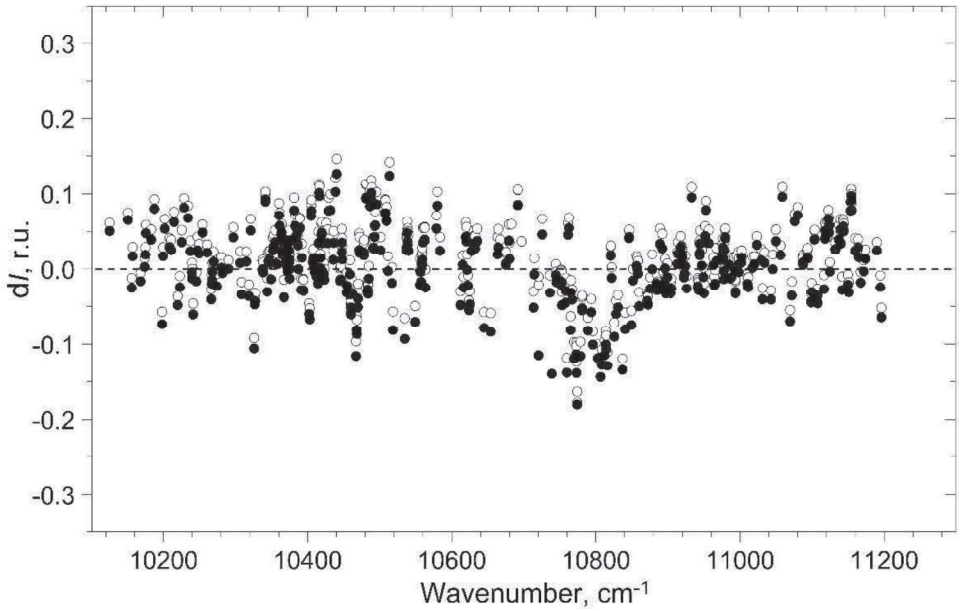

Fig. 2. Relative deviation of line intensities in the spectral region under investigation for measurements at 431K and 2070 mbar: empty circles – before pressure adjustment (2039 mbar), black points – after pressure adjustment (increased by 1.5%).

4. Retrieval of the water vapour continuum absorption

At the first stage of the analysis, the water vapour continuum optical depth $\tau_\mathrm{c}(\nu)$ was derived as a difference between the experimental optical depth spectrum $\tau(\nu)$ (see Section 2) and the cumulative local contribution of water monomer lines $\tau_\mathrm{mon}(\nu)$ calculated with the line-by-line technique [34]. An example of the preliminary retrieval of the continuum absorption is given in Fig.3 (grey points). Fluctuations of the continuum at frequencies corresponding to water monomer line centres are caused by uncertainties in spectral line parameters. Generally, the retrieval of the continuum is not possible at line centres within absorption bands, because the continuum component is much less (2 orders of

magnitude) than the line contribution. Even small relative errors in line parameters lead to large errors in the retrieved continuum. Therefore, the continuum absorption can only be derived in the microwindows between absorption lines (blue points in Fig. 3), where the impact of uncertainties in line parameters on the retrieved continuum is often relatively small (less than 10–20%). The exclusion of line centres from the continuum retrieval does not lead to significant information loss since the continuum possesses a rather smooth spectral character within several halfwidths of a spectral line. Moreover, spectral smoothing was applied to select the most reliable continuum information within these microwindows – the continuum data points were obtained by averaging over ten data points, corresponding to a derived continuum at a spectral resolution of between 1 to 4 cm^{-1} depending on the measurement pressure. This procedure helps to exclude false minima in the experimental spectrum within microwindows. An example of the retrieved continuum spectrum including smoothing is shown by the red points in Fig. 3. In the remainder of this paper, this smoothed continuum is used throughout. The semi-empirical MT_CKD-3.2 continuum model [33] is also shown (dashed line in Fig.3) for the measurement conditions.

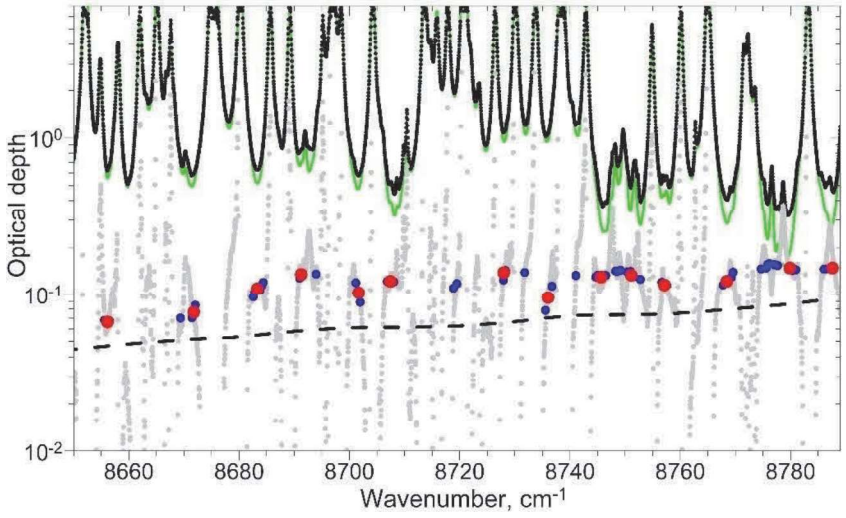

Fig. 3. Example of the continuum absorption spectrum retrieved from the experimental data (431K, 1080 mbar): measured absorption spectrum of pure water vapour($\tau(\nu)$, black points), MT_CKD-3.2 model (dashed line), calculated spectrum of the local line absorption $\tau_{mon}(\nu)$ without the "CKD plinth" (green line), difference between the measured water vapour absorption and calculated local lines monomer absorption ($\tau(\nu) - \tau_{mon}(\nu)$, grey points), the differential spectrum $\tau(\nu) - \tau_{mon}(\nu)$ after filtering (blue points), smoothed continuum spectrum $\tau_c(\nu)$ (red points).

The self-continuum cross-section $C_s(\nu,T)$ in units of $cm^2molec^{-1}atm^{-1}$ was derived using the equation

$$C_s(\nu,T) = \frac{\tau_c(\nu)}{\rho_s P_s L} = \tau_c(\nu)\frac{kT}{P_s^2 L} = \alpha(\nu)\frac{kT}{P_s^2} \qquad (2)$$

where ρ_s and P_s are water vapour number density and pressure, respectively, k is the Boltzmann constant, T is temperature and L is the optical path length, $\alpha(\nu)$ is the absorption coefficient. Figures 4 (a,b) illustrate the close agreement of cross-sections obtained from a range of pressures at both temperatures (398 and 431 K).

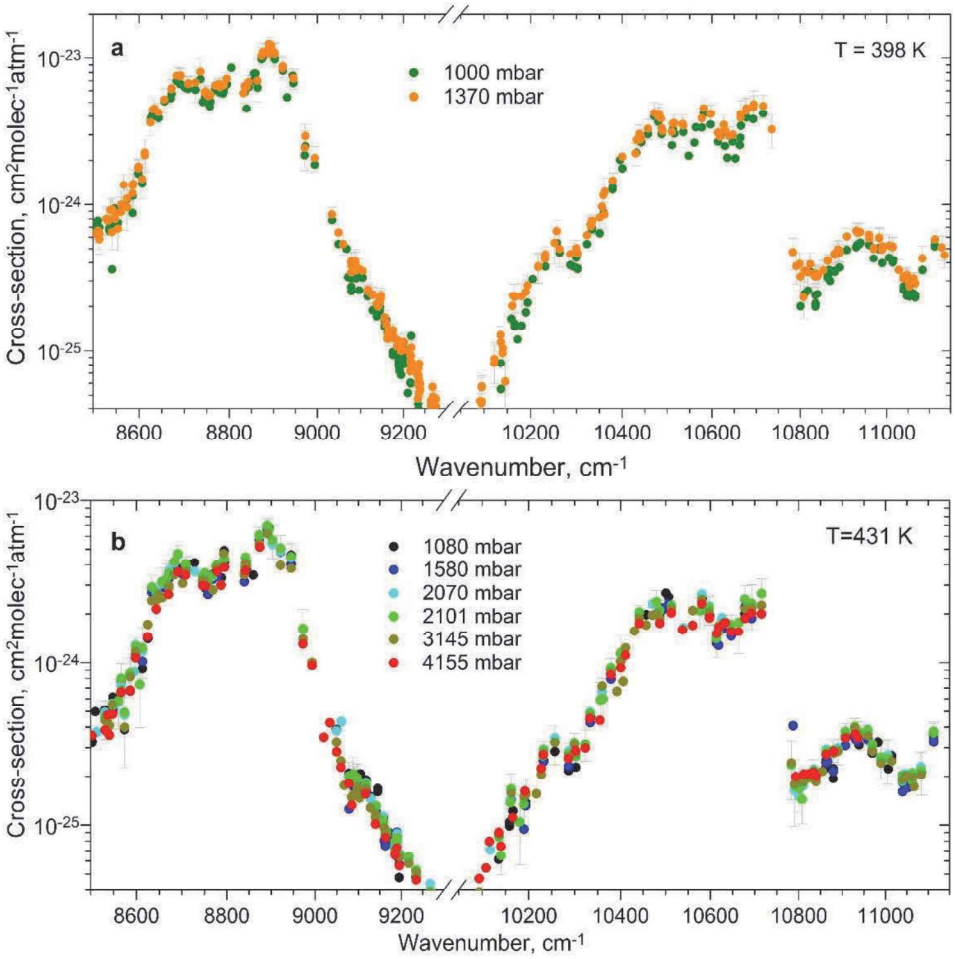

Fig. 4. Cross-section spectra of the water vapour continuum absorption obtained using eq. (2) for two pressure sets:1000 and 1370 mbar at 398 K (**a**) and six pressures from 1080 to 4155 mbar at 431 (**b**) K. The error bars are given for the continuum cross-section spectra corresponding to 1370 mbar, 398 K (**a**), and 2101 mbar, 431 K (**b**).

A linear fitting was performed to confirm the pressure-squared dependence of the measured water vapour continuum absorption. The continuum absorption coefficients $\alpha(v)$ *versus* P^2 are presented in Fig.5 for some microwindows. There is good agreement between the experimental points and the fitted linear function ($y=kx+b$) and the intercept b is always close to zero. This helps confirm the quality of the observations. The slope of the straight line determines the cross-section value (Fig.6). Figure 6 demonstrates the expected inverse temperature dependence of the retrieved continuum absorption.

The retrieved self-continua within the 8800 and 10600 cm^{-1} absorption bands demonstrates the presence of several spectral peaks that are absent in the MT_CKD-3.2 continuum model (dashed lines in Fig.6), although the MT_CKD-3.2 represents the overall shape of the continuum absorption quite satisfactorily. Similar peaks were previously reported within more intense near-IR water vapour absorption bands [9]. It is also apparent that the MT_CKD-3.2 model underestimates the observed continuum by about 1.5–2 times on average at the investigated temperatures in the centre of the bands (see lower panel of Fig. 6). The data at 11084 and 11113 cm^{-1} wavenumbers demonstrate the greatest deviation from MT_CKD-3.2 and may reflect the beginning of the q-dimer subband in the continuum spectrum (see Fig. 9 and further discussion in Section 6). However, it was not possible to retrieve this spectral feature completely since the difference between the experimental data and the calculated contribution of water monomers turned out to be too noisy.

We acknowledge that MT_CKD was not designed for application at such high temperatures, as it was intended for use in atmospheric conditions, although as noted in Section 1, the temperature dependence was defined using measurements at elevated temperatures at lower wavenumbers.

As a consequence of the above arguments, our measurements clearly indicate limitations in the MT_CKD model in this spectral region and at these temperatures. A more physically-based model of the water vapour continuum is now required to address the limitations highlighted here. Such a model should include significant advances in experimental and theoretical capabilities, and to have a quite wide range of applicability beyond the conditions (both spectral and temperature) for which it was derived.

The cross-sections of the water vapour self-continuum absorption, obtained here for the first time from laboratory measurements at elevated temperatures, are given in Appendix 1.

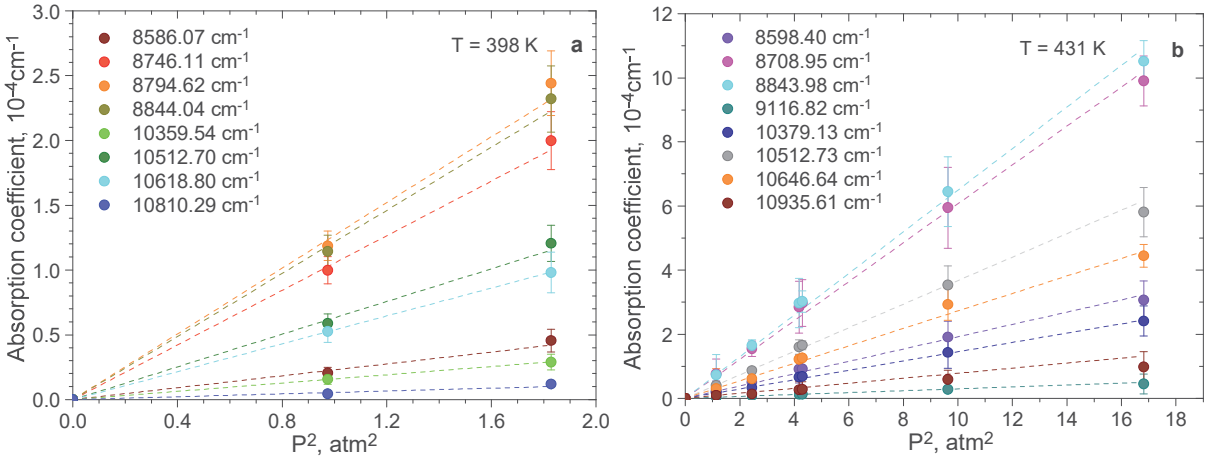

Fig. 5. Examples of P^2 dependence of the retrieved self-continuum absorption coefficients in some microwindows at 398 (**a**) and 431 (**b**) K.

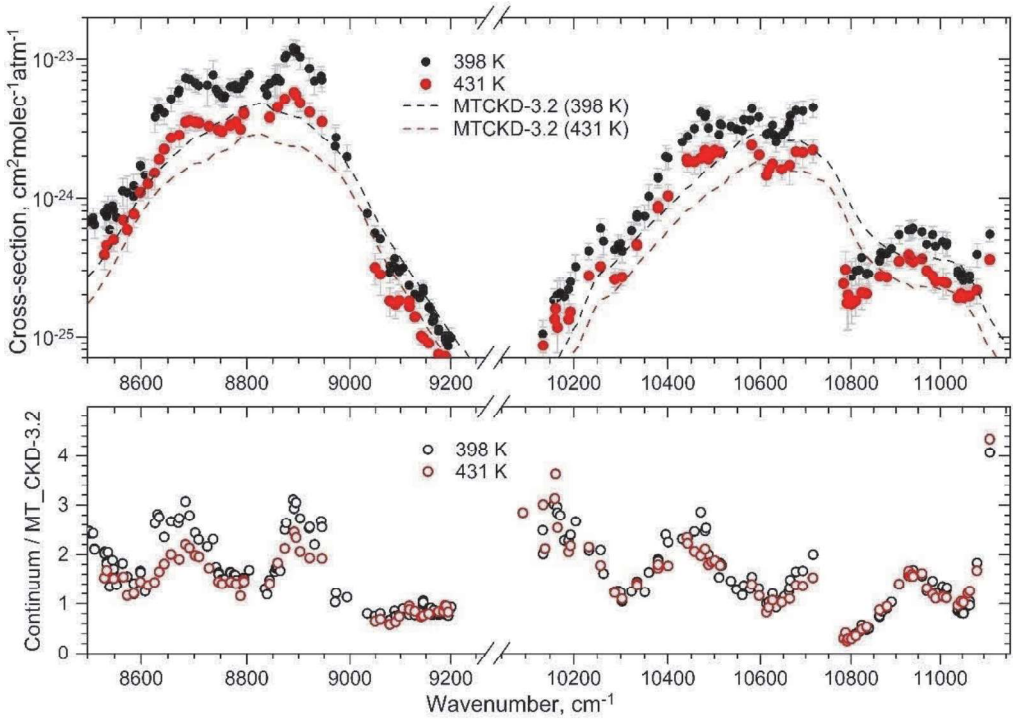

Fig. 6. Cross-section spectra of the water vapour self-continuum absorption retrieved from the experiment (upper panel) at 398 K (blue) and 431 K (red). The dashed lines show the corresponding MT_CKD-3.2 model spectra. Respective ratios of the derived continuum to the MT_CKD-3.2 model are shown in the bottom panel.

5. Simulation of water dimer absorption spectra

It has been shown in [7–9,20] that the spectral features of the water vapour self-continuum absorption within near-IR spectral bands are likely caused by a significant contribution from water dimers. In our study, the parameterization of the dimer model proposed in [9] was used for the 8800 and 10600 cm^{-1} absorption bands. The total water dimer absorption cross-section (b-dimers + q-dimers) C_s (in [cm^2/atm/molec], where 'atm' and 'molec' applies to the pressure and number of water monomers, respectively) was simulated using the following equation:

$$C_s(\nu) = K^b_{eq} \sum_i S^b_i f^b_i(\Delta\nu_i, \gamma^b) + K^q_{eq} \sum_j S^q_j f^q_j(\Delta\nu_j, \gamma^q), \quad (3)$$

where K^b_{eq} and K^q_{eq} are the equilibrium constants of b- and q-dimers (in [atm^{-1}] ≡ [$n_{dimers}/n_{monomers}$ per 1 atm of water monomers]); S^b_i is the intensity of i-th subband of b-dimers [cm/dimer]; S^q_i is the intensity of i-th line of q-dimers [cm/dimer]; $f^b_i(\Delta\nu_i,\gamma^b)$ and $f^q_i(\Delta\nu_i,\gamma^q)$ are Voigt profiles [cm] with halfwidths at half-maximum intensity γ^b and γ^q [cm^{-1}] of b- and q-dimers, respectively; $\Delta\nu_i$ is the distance from the centres of b-dimer subbands; $\Delta\nu_j$ [cm^{-1}] is a distance from q-dimer line centre. The calculation was carried out using the LBL_{IAO} line-by-line program [34]. It is important to note that all parameters in Eq.(3) have a clear physical meaning as opposed to the semi-empirical parameters that are often used in continuum models.The physical background of the model parameters – and so, the possibility to verify them from other sources – will allow us (similar to that in [24,39]) to estimate the contribution of water dimers to the continuum absorption in the investigated bands (see Section 6). In Section 7 (devoted to the atmospheric calculations), we will use this relatively simple dimer model to extrapolate the self-continuum from 400-430 K to the 260-296 K temperature range.

Some data on the frequencies and strengths of several main bending and stretching oscillations in b-dimers can be obtained from theoretical calculations and low-temperature measurements [28,40–42]. In this work, the b-dimer spectrum was simulated on the basis of quantum-chemical calculations of the O-H stretching vibrational overtone spectrum of the water dimer presented as two individually vibrating monomer units [29]. The used data for the intensities of b-dimer transitions is presented in Table 2. The Voigt profile with 20 cm^{-1} halfwidth was used to simulate the subbands shape of b-dimers, as it fits best the respective experimental features. However, this parameter has a minor effect on the total water dimer spectrum (absorption by b- and q-dimers), since b-dimers contribute weakly to the water vapour self-continuum at high temperatures within the bands investigated here (see details below). Recently interpreted measurements [43] of the self-continuum in the 3600 cm^{-1} band at 296 K used a more sophisticated, although still speculative, approach to modelling the b-dimer band shape. This is based on estimates of the b-dimer rotational constants and distinguishing between parallel and perpendicular bands; at this lower temperature, the contribution of b- and q-dimers is expected to be more equal, so that assumptions on the b-dimer shape are more important than is the case here.

Table 2. Positions and intensities of transitions in bound dimer [29] used for the water dimer model.

Local mode assignments*	Wavenumber, cm^{-1}	Intensity, cm/molec
$\|0\rangle_f\|2\rangle_b\|1\rangle$	8530.5	2.35E-21
$\|20\rangle_+\|1\rangle$(70%)+$\|11\rangle_+\|1\rangle$(16%)	8754.9	6E-22
$\|2\rangle_f\|0\rangle_b\|1\rangle$(63%)+$\|1\rangle_f\|1\rangle_b\|1\rangle$(22%)	8804.8	7E-21

$\|20\rangle_.\|1\rangle$	8806.9	5.5E-20
$\|1\rangle_f\|1\rangle_b\|1\rangle$(66%)+$\|2\rangle_f\|0\rangle_b\|1\rangle$(25%)	8930.1	1.9E-21
$\|11\rangle_+\|1\rangle$(74%)+$\|20\rangle_+\|1\rangle$(18%)	9006.9	4.85E-24
$\|0\rangle_f\|2\rangle_b\|2\rangle$(69%)+$\|0\rangle_f\|3\rangle_b\|0\rangle$(13%)	10057.5	2.65E-22
$\|0\rangle_f\|3\rangle_b\|0\rangle$(80%)+$\|0\rangle_f\|2\rangle_b\|2\rangle$(12%)	10161.1	1.95E-21
$\|30\rangle_+\|0\rangle$(77%)+$\|21\rangle_+\|0\rangle$(9%)	10601	1.85E-21
$\|3\rangle_f\|0\rangle_b\|0\rangle$(67%)+$\|2\rangle_f\|1\rangle_b\|0\rangle$(12%)	10611	6.5E-21
$\|30\rangle_.\|0\rangle$	10615.3	1.8E-20
$\|1\rangle_f\|2\rangle_b\|0\rangle$(68%)+$\|3\rangle_f\|0\rangle_b\|0\rangle$(15%)	10673.7	9.5E-21
$\|21\rangle_+\|0\rangle$(80%)+$\|30\rangle_+\|0\rangle$(10%)	10869.7	8E-22
$\|2\rangle_f\|1\rangle_b\|0\rangle$(74%)+$\|1\rangle_f\|2\rangle_b\|0\rangle$(15%)	10889.1	3.5E-21
$\|21\rangle_.\|0\rangle$	11042	2.25E-21

* According to the notation [28], $|x\rangle_f|y\rangle_b|z\rangle$ and $|xy\rangle_\pm|z\rangle$label the vibrational modes in the donor and acceptor water unit respectively. Here, x and y denote number of the vibrational quanta respectively in the free ('f') and bound ('b') OH-stretching mode in the donor unit, z is the quanta in the H_fOH_b bending mode, while "±" refers to the symmetry of the stretching vibrations in the acceptor unit.

Quasibound dimers, which can be considered as a transitional state between free-pairs and b-dimers, have not been studied as much as the bound states. Therefore, a very simple approximate model of q-dimer lines was used here. In a similar way to [9], the q-dimer absorption spectrum was simulated as a sum of strongly broadened water monomer lines with doubled intensity S_i (i.e. $S^q_i = 2S_i$). Strong broadening occurs because the lifetime of q-dimers is rather short (~10^{-12} s). The halfwidth of q-dimer lines was set to 10 cm^{-1}, which corresponds to estimates of their average lifetime (see [9]). Intensities of q-dimer lines were assumed to be equal to double the intensities of the corresponding water monomer lines, as an approximation for two slightly interacting water monomers in a short-lived metastable state. For simulation of the q-dimer spectrum, intensities and centres of monomer lines were taken from the HITRAN-2016 database [35]. It was shown that the total dimer spectrum agrees well with the measured continuum within 1600 and 3600 cm^{-1} absorption bands [9] despite using this quite simple model for the description of the q-dimer spectrum.

The main challenge in parameterization of the dimer model (Eq. (3)) is to determine the equilibrium constant of q-dimers. Direct quantum-chemical calculations of this value, especially for the high temperatures observed here, are not available at present. In this work, an attempt was made to derive both K^b_{eq} and K^q_{eq} values by fitting the model (Eq. (3)) to the retrieved continuum within 8800 and 10600 cm^{-1}absorption bands. As a result, a satisfactory spectral agreement between the dimer model and the continuum absorption spectrum was established. A significant difference in the expected contribution of b- and q-dimers at the measurement temperatures was also observed, with a strong prevalence of q-dimers. This result supports the conclusion made on the basis of the statistical approach [19,21] for the temperature dependence of K^b_{eq} and K^q_{eq}. However, K^b_{eq} values derived from this fitting were characterized by significant estimated errors that exceed 100% in some cases. This is due to the very small relative contribution of b-dimers to the total absorption at the investigated temperatures, so that a simultaneous fitting of b- and q-dimer spectra to the continuum leads to large estimated errors in the derived K^b_{eq} values and in the fitting itself.

Currently two relatively recent independent estimates of K^b_{eq} temperature dependence are available [40,41]. The first [40] requires recalculation adjusted for a more accurate value of the dissociation energy obtained from measurements [44] (D_0^{new} = 1105 cm^{-1} instead of D_0=1234 cm^{-1} used in [40]). In our work, the adjusting factor $e^{(D_0^{new}-D_0)/kT}$ was applied to K^b_{eq} from [40]. The available calculated temperature dependences of K^b_{eq} (Fig.7, red [40] (modified) and black [41] (with D_0 = 1105 cm^{-1}) solid curves) noticeably differ from each other at low temperatures. Moreover, both estimatesare partially confirmed by different experimental data at temperature up to 350 K (see, for example, Fig.6 (left panel) in [24]). Therefore, in the next step, the average value of these two

estimates (further denoted as $K^{b(aver)}_{eq}$) was taken for simulation of b-dimer absorption spectra. Table 3a contains the model parameters for b-dimer spectra calculation. Thus, the main fitting parameter of the dimer model was the q-dimer equilibrium constant. Table 3b (column 5) presents the obtained K^{q}_{eq} values as a result of fitting the dimer model (Eq. (3)) to the retrieved continuum spectra with $K^{b(aver)}_{eq}$ values from theoretical calculations (Table 3a, column 5) using the least square method. The rms deviation of K^{q}_{eq} is 29% on average.

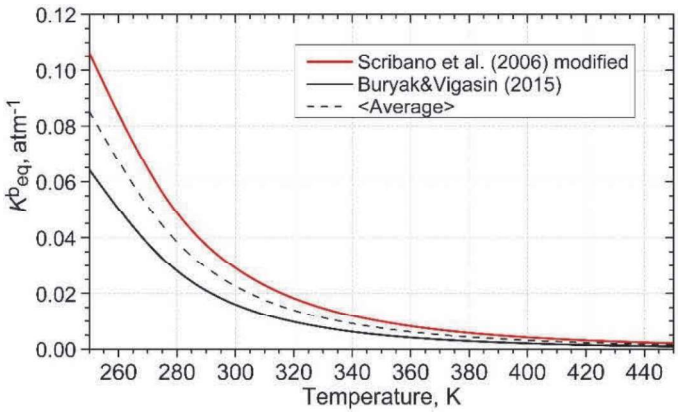

Fig. 7. Temperature dependence of b-dimer equilibrium constant obtained in *ab initio* calculations [40] and modified for D_0 (see the text above) (red curve), and in [41] (black solid curve). The average values between [40] modified and [41] are shown by dashed black curve.

Table 3. Result of the dimer model parameterization:

a – Parameters for simulating b-dimer absorption spectra using theoretical calculations for equilibrium constant K^{b}_{eq} (see details above).

Temperature, K	Absorption band, cm^{-1}	Intensities and centre positions	Subband HWHM, γ, cm^{-1}	$K^{b(aver)}_{eq}$, atm^{-1}
398	8800, 10600	Quantum-chemical calculations [29]	20	0.0031
431	8800, 10600			0.0019

b– Parameters for simulating q-dimer absorption spectra using fitted values (5th column) and theoretical calculations for equilibrium constant K^{q}_{eq} (column 6, see Section 6).

Temperature, K	Absorption band, cm^{-1}	Intensities and centre positions	Line HWHM, γ, cm^{-1}	$K^{q(fit)}_{eq}$, atm^{-1}	$K^{q(calc)}_{eq}$, atm^{-1}
398	8800	Strongly broadened monomer lines from HITRAN-2016 [35] with doubled monomer intensities	10	0.0306	0.0090
	10600			0.0284	
431	8800			0.0170	0.0069
	10600			0.0168	

6. Discussion

As mentioned earlier, there is no direct information about the q-dimer equilibrium constant at present, but it can be roughly estimated using information about the b-dimer and the total equilibrium constants as defined by Eq. (4)

$$K^{b+q}_{eq} = K^{b}_{eq} + K^{q}_{eq}. \qquad (4)$$

Currently, three estimates of the total equilibrium constant K^{b+q}_{eq} are known from different approaches to determine the second virial coefficient [45,46] and from the thermodynamic properties of water dimers [47]. These data can be considered reliable as they are in good agreement with each

other (see Fig.8, solid grey, solid black, and dash-dot black curves). In this work, we apply the temperature dependence of K^{b+q}_{eq} derived from the virial equation of state for real gases, using highly accurate measurements of water vapour thermodynamic properties [45]. The difference between K^{b+q}_{eq} [45] and $K^{b(aver)}_{eq}$ was taken to get approximate temperature dependence of $K^{q(calc)}_{eq}$ (see black dashed curve in Fig.8 and values in column 6 of Tab.3b). Column 5 in Tab.3b contains the values of $K^{q(fit)}_{eq}$ obtained as a result of the dimer model fitting to the retrieved water vapour self-continuum spectra.

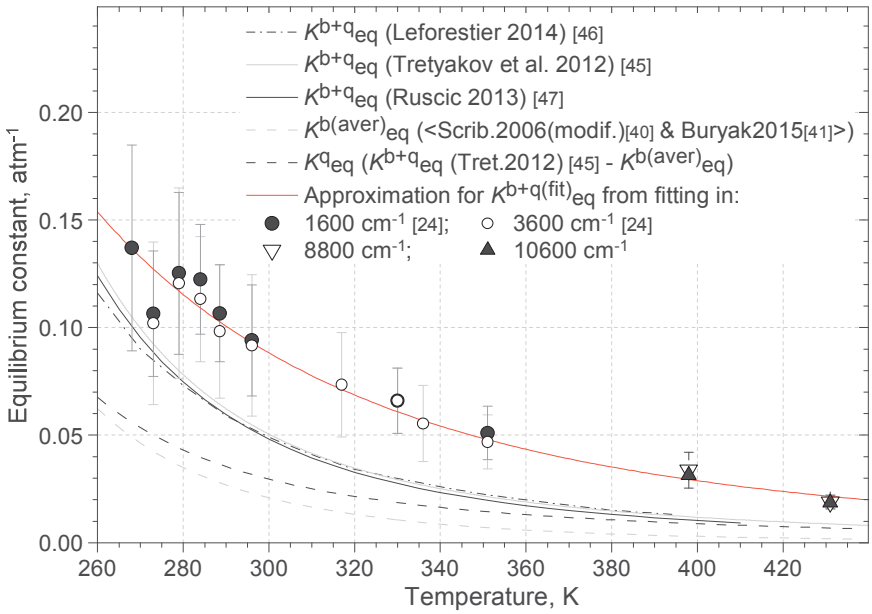

Fig. 8. Temperature dependences of equilibrium constants obtained from different approaches: total equilibrium constant K^{b+q}_{eq} obtained from quantum-chemical calculation [46] (dash-dot curve), from the second virial coefficient [45] (solid grey curve), and thermodynamic properties of water dimers [47] (solid black curve); average values of b-dimer equilibrium constant $K^{b(aver)}_{eq}$ [40] (modified) and [41] (grey dashed curve); q-dimer equilibrium constant $K^{q(calc.)}_{eq}$ obtained in this work as a difference between K^{b+q}_{eq} [45] and $K^{b(aver)}_{eq}$ (black dashed curve); total equilibrium constant K^{b+q}_{eq} obtained from the fitting of the dimer model to experimental water vapour continuum spectra within 1600 and 3600 cm^{-1} bands (black and white circles) [24]; K^{b+q}_{eq} obtained from the fitting within 8800 and 10600 cm^{-1} bands (white and black triangles) in the current work; approximation function of all experimental points for the total equilibrium constant derived using the water dimer continuum model [9] within the near-IR absorption bands (solid red curve).

The values of $K^{q(fit)}_{eq}$ obtained from fitting the dimer model (Eq. (3)) to the experimental continuum in two different absorption bands at each temperature are close to each other (see triangle symbols in Fig. 8). This seems a reliable result as the concentration of water dimers (characterized by an equilibrium constant) in water vapour should not depend on the spectral region. The examples of fitting the dimer model (3) to the experimental data are presented in Fig.9 (a,b,g,h). Given the very approximate character of the q-dimer absorption model (the second term in Eq. (3)) and the dominant contribution of q-dimers at the investigated temperatures, the dimer model provides a fairly detailed spectral description of the retrieved self-continuum spectra.

Comparison of values in columns 5 and 6 in Tab. 3b shows evidence that the fitted values $K^{q(fit)}_{eq}$ are significantly greater than $K^{q(calc)}_{eq}$ derived from Eq. (4) using reliable values, by about a factor of 3 on average. A more complete picture of the dimer model parameterisation can be seen in Fig.8. The total equilibrium constant K^{b+q}_{eq} data obtained at relatively low temperatures within 1600 and 3600 cm^{-1} bands [24] and at elevated temperatures within 8800 and 10600 cm^{-1} absorption bands was interpolated in this work using the empirical fit

$$K_{eq}^{b+q}(T) = 3.717 \cdot 10^{8} \cdot T^{-3.886}. \quad (5)$$

This can be considered as the temperature dependence of some *effective* total dimerization constant (solid red curve in Fig. 8); i.e. it is the constant that gives a satisfactory description of spectral behaviour and strength of the water vapour self-continuum in the investigated spectral regions, irrespective of the physical origin of the continuum (see upper panels at each temperature (a,b,g,h) in Fig.9) if the intensities of the b- and q-dimer used here are assumed to be correct and no other mechanisms were responsible for the continuum. We refer to the dimer model using this empirical fit as the "dimer-based model".

The effective equilibrium constant $K^{b+q(fit)}_{eq}$ obtained in this work is a factor of 1.5-2.5 greater than values of K^{b+q}_{eq} from prior estimates [45–47] across the entire temperature range. This means the best fitting of the dimer model (Eq. (3)) requires a larger quantity of water dimers than can be objectively explained at the considered thermodynamic conditions (according to the independent estimates), and it is K^{q}_{eq} that is strongly overestimated in our model. One possible explanation of this result can be a contribution from additional mechanisms for the water vapour self-continuum which is not accounted for in our model. For example, it could be absorption by intermediate line wings as suggested in [39]. The recent analysis [43] of measurements in the 3600 cm^{-1} band at 296 K reached a broadly similar conclusion, finding a factor of about 1.35 greater $K^{b+q(fit)}_{eq}$ (which is within the uncertainty at 296 K shown in Fig. 8) than expected from the prior estimates; they also suggested that enhanced absorption in the intermediate wings [39] may explain the difference. Another explanation could be overestimation of the intensities of fundamental transitions of the b-dimers in [29] caused by the neglect of intermolecular vibrations in the dimer model. Inclusion of the intermolecular modes into quantum-chemical calculations may potentially decrease the intensity of fundamental transition (the main spectral peaks) up to 30% [48,49], but strongly increase the calculated underlying part of b-dimer absorption which is currently mostly attributed to the q-dimers by the fitting procedure. It should be stressed that it is more likely that an overestimation of $K^{q(fit)}_{eq}$ in our current fitting that leads to the overestimation of the total $K^{b+q(fit)}_{eq}$.

Fig. 9 (c,d,i,j) contains the simulated water dimer absorption spectra using the values of $K^{b(aver)}_{eq}$ (Table 3a, 5 column) and $K^{q(calc)}_{eq}$ (Table 3b, column 6) obtained from Eq. (4). The integrated spectral contribution of the b-dimer and q-dimer absorption to the continuum is 36% at 398 K and 45% at 431 K in this case. The part of the retrieved continuum that is unexplained by water dimers using the currently-available theory, and total equilibrium constant, is presented in Fig. 9 (e,f,k,l).

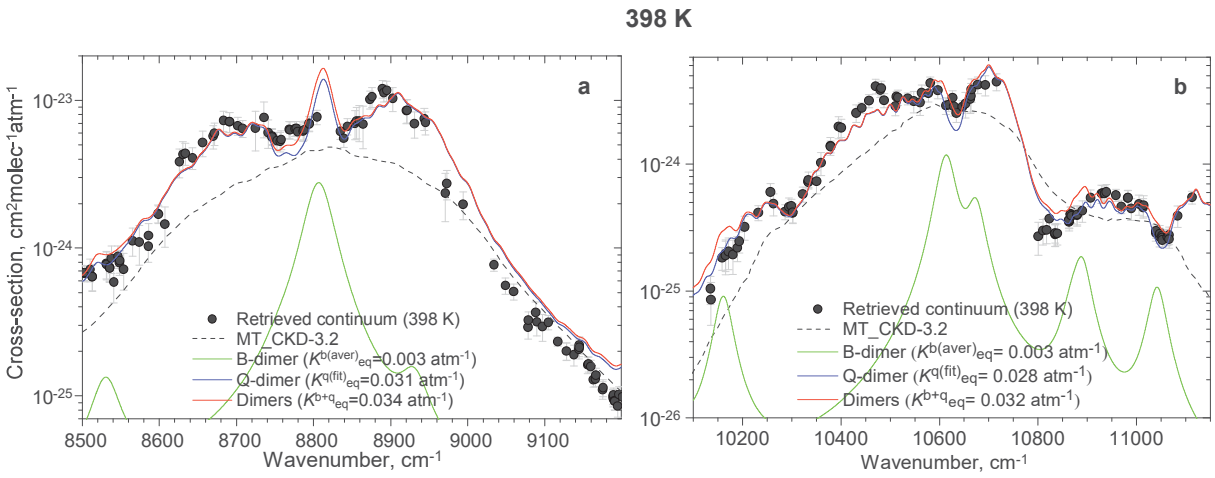

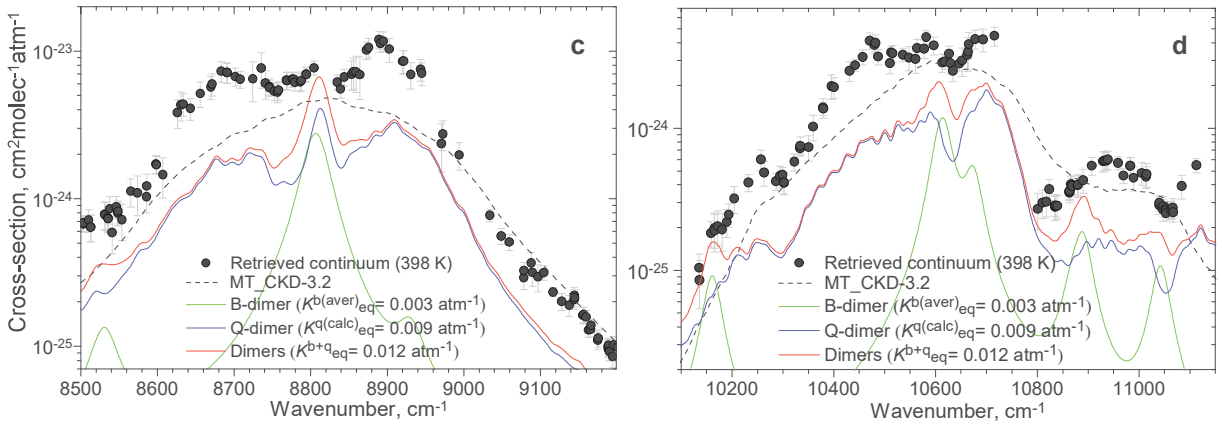
c
d
Cross-section, cm²molec⁻¹atm⁻¹
Wavenumber, cm⁻¹
Retrieved continuum (398 K)
MT_CKD-3.2
B-dimer ($K^{b(aver)}_{eq}$= 0.003 atm⁻¹)
Q-dimer ($K^{q(calc)}_{eq}$= 0.009 atm⁻¹)
Dimers (K^{b+q}_{eq}= 0.012 atm⁻¹)

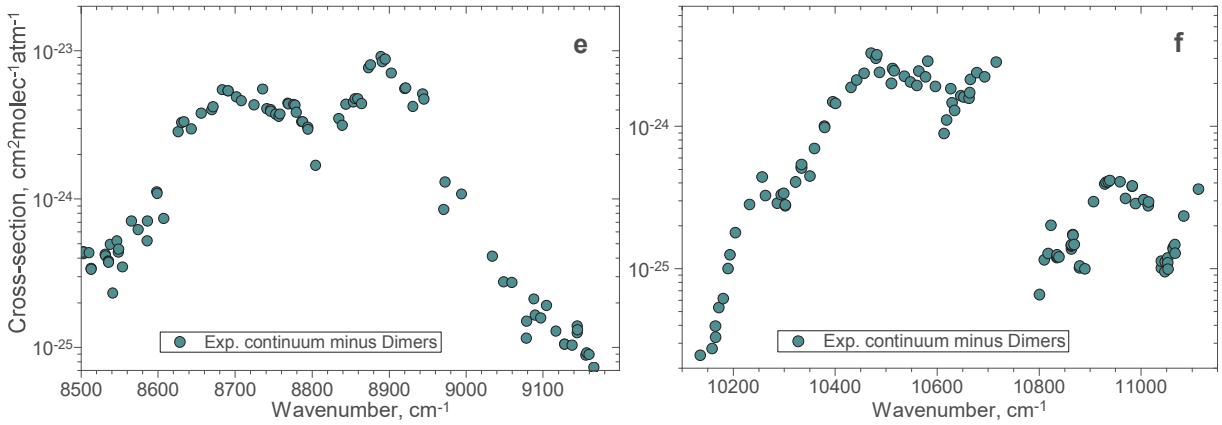
e
f
Cross-section, cm²molec⁻¹atm⁻¹
Wavenumber, cm⁻¹
Exp. continuum minus Dimers

431 K

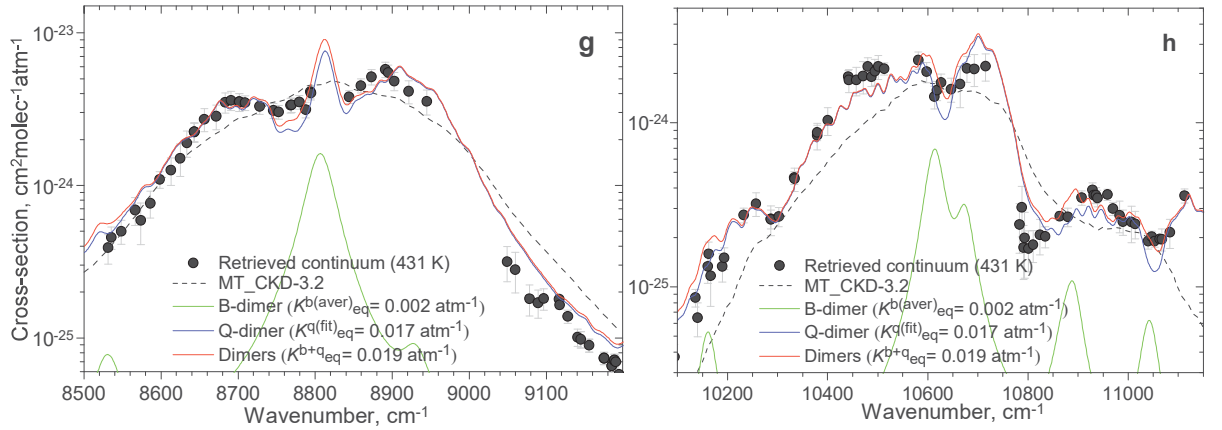
g
h
Cross-section, cm²molec⁻¹atm⁻¹
Wavenumber, cm⁻¹
Retrieved continuum (431 K)
MT_CKD-3.2
B-dimer ($K^{b(aver)}_{eq}$= 0.002 atm⁻¹)
Q-dimer ($K^{q(fit)}_{eq}$= 0.017 atm⁻¹)
Dimers (K^{b+q}_{eq}= 0.019 atm⁻¹)

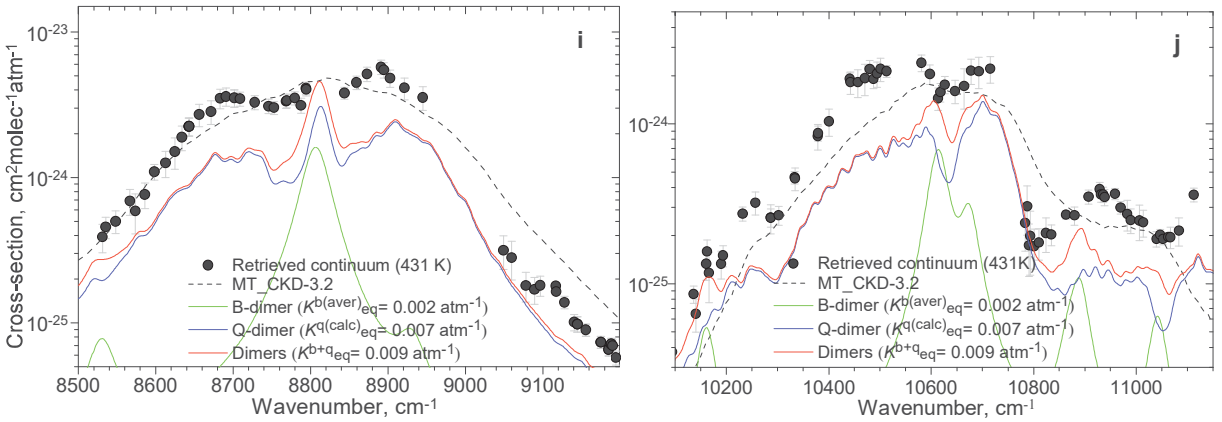
i
j
Cross-section, cm²molec⁻¹atm⁻¹
Wavenumber, cm⁻¹
Retrieved continuum (431 K)
MT_CKD-3.2
B-dimer ($K^{b(aver)}_{eq}$= 0.002 atm⁻¹)
Q-dimer ($K^{q(calc)}_{eq}$= 0.007 atm⁻¹)
Dimers (K^{b+q}_{eq}= 0.009 atm⁻¹)

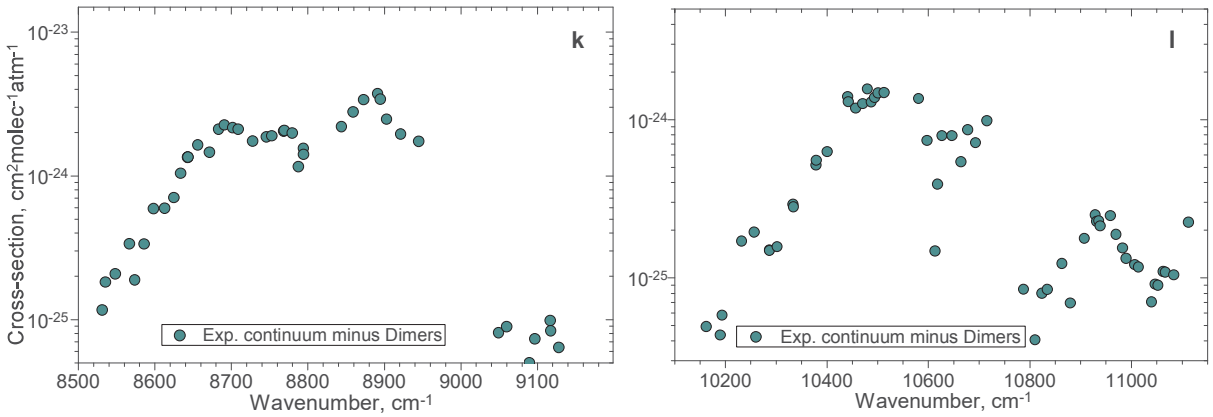

Fig. 9. Result of the water dimer model (Eq. (3)) fitting within the 8800 cm^{-1} (left panels) and 10600 cm^{-1} (right panels) absorption bands at 398 K (a-d) and 431 K (g-j). Upper panels at each temperature: the result of the water dimer model fitting to the retrieved water vapour self-continuum cross-section spectra using the fitting parameter $K^{q(fit)}_{eq}$. Middle panels at each temperature: the result of the water dimer model simulation using theoretically-derived estimated values $K^{b(aver)}_{eq}$ and $K^{q(calc)}_{eq}$. Lower panels (e,f at 398 K and k,l at 431 K): the unexplained part of the continuum absorption obtained as a difference of the retrieved continuum and the dimer model from middle panels (c,d at 398 K and i,j at 431 K). The water vapour self-continuum spectrum derived from measurements (black circles), model spectra of b- and q-dimers (green and blue curves, respectively), total model spectrum of water dimers (red curve), MT_CKD-3.2 model (dashed curve), the unexplained absorption spectrum (dark green circles). The parameter values of the water dimer model are given in Tab. 3 a,b.

7. Radiative impact of the new self-continuum

This section aims to determine how much of an effect the retrieved water vapour self-continuum absorption has from the perspective of atmospheric radiative transfer. Within the investigated 8800 and 10600 cm^{-1} absorption bands, water vapour lines and the self-continuum are weaker than in the bands at lower wavenumbers. The near-visible absorption bands, unlike the stronger near-IR bands, do not completely attenuate solar radiation between the top-of-atmosphere and the surface layer (i.e. their absorption is not saturated); therefore, uncertainty in absorption within these bands has more impact on the calculated shortwave surface fluxes than near-IR bands at lower wavenumbers.

Despite the fact that our observations are limited by the elevated temperatures (398 and 431 K), the good agreement between the experimentally-retrieved water vapour continuum and the dimer-based model (see Fig. 9, a,b,g,h) allows us to simulate H_2O self-continuum spectra at atmospheric temperatures by extrapolating the dimer-based model. Here, for the temperatures of interest, we calculated the water dimer cross-sections (Eq. (3)) with the effective values of K^{b+q}_{eq} obtained from the best fit to the experimental data at different temperatures and approximated using the temperature dependence from Eq. (5). Figure 10 shows the extrapolated coefficients from the dimer-based model at 296 and 260 K (see Supplementary materials 3), compared to those from MT_CKD-3.2 at the same temperatures. Despite MT_CKD-3.2 being a factor of ~1.5-2 weaker on average than the observed continuum at elevated temperatures, at atmospheric temperatures there is reasonable agreement between the dimer-based model (using the effective value of K^{b+q}_{eq}) and MT_CKD-3.2. However, this agreement must be treated with caution, as the true temperature dependence in these bands, strictly speaking, may be different to that obtained from the combination of these and near-IR bands at different temperatures (Fig. 8 and Eq. (5)) – we do not have direct observational evidence that this is the case. Also, the dimer model and MT_CKD-3.2 demonstrate different spectral behaviour; the dimer-based model has various peaks and troughs corresponding mainly to the

transitions of the q-dimer, and there are also some larger differences at the edges of each of the two bands.

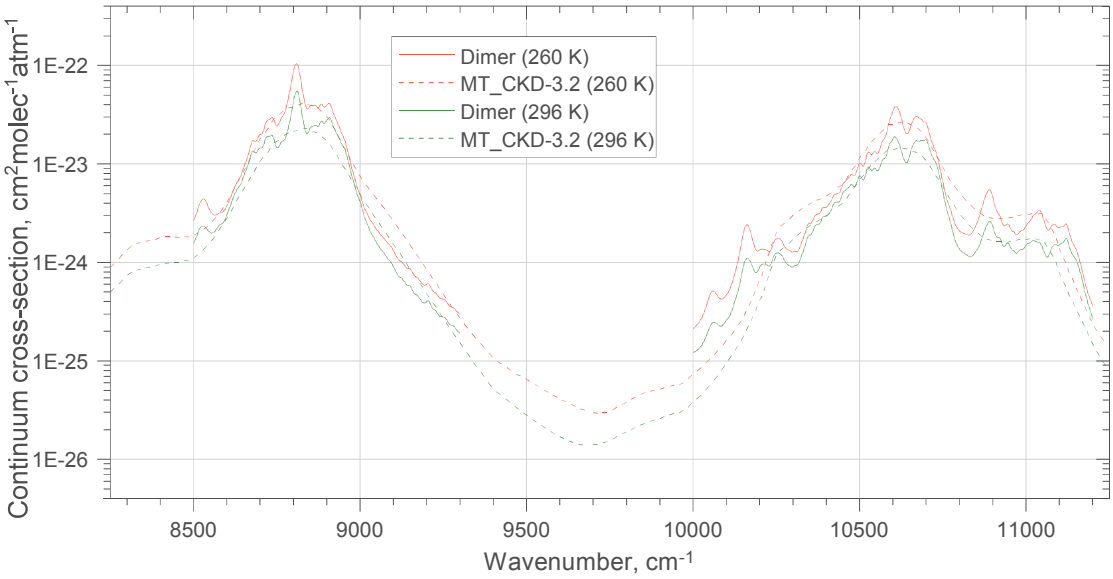

Fig. 10 MT_CKD-3.2 (dashed lines) and dimer-based model coefficients (solid lines) at 260 K (red) and 296 K (green).

We derived the dimer-based model spectrum at 296 and 260 K, which are the temperatures at which the MT_CKD continuum coefficients are specified. For ease of incorporation into our radiative transfer model, we then use the MT_CKD temperature dependence to interpolate the dimer absorption between these temperatures. The MT_CKD temperature dependence is of the form

$$C_s(\nu,T) = Cs(\nu,T_0)\left(\frac{C_s(\nu,T_1)}{C_s(\nu,T_0)}\right)^{(T-T_0)/(T_1-T_0)}, (6)$$

where T_0 is 296 K and T_1 is 260 K. Since this temperature dependence interpolates absorption cross-sections between 296 and 260 K, and the dimer-based model shows a reason able agreement with MT_CKD at these two temperatures (Fig. 10), one can expect that the temperature dependences of these two models do not deviate significantly in this temperature region. The highest tropospheric temperature used in our model atmospheres is 300 K, meaning that the MT_CKD temperature dependence is suitable for modelling the range of temperatures we explore here (260-300 K); at 280 K the difference is no more than 3% at any wavenumber, and averages out to 0.15%.

To estimate irradiances, we use an updated version of the RFMDISORT radiative transfer tool (used, for example, in [50]). This is a combination of two established radiative transfer codes; the Reference Forward Model [51] (a line-by-line code used to determine gas absorption) and DISORT [52] (a multiple scattering code used to compute irradiances). A spectral resolution of 0.1 cm^{-1} is used here. We use an offline version of MT_CKD-3.2 to calculate continuum absorption, with modifications using user-provided continuum absorption cross-sections. For this work, we used tropical (TRO), mid-latitude summer (MLS) and sub-arctic winter (SAW) standard atmospheres, with specified profiles of H_2O, CO_2 (at 380 ppmv), CH_4 (1.7 ppmv), O_2, N_2 and O_3. Spectral data is obtained from the HITRAN2016 database. We used the Kurucz solar spectral irradiance [53]. These calculations are for clear-sky conditions, and include the effects of Rayleigh scattering, with a spectrally constant surface albedo of 0.3. For an overhead Sun, the original MT_CKD-3.2 self-continuum reduces the downwelling surface irradiance by ~ 0.26 W m^{-2} in MLS conditions compared to the no-continuum case across the 8500-9250 cm^{-1} and 10000-112000 cm^{-1} bands (see Fig.11 (c, d)). This value is strongly dependent on the humidity; for SAW the absorbed irradiance is as low as

~0.014 W m^{-2}, but as high as ~0.46 W m^{-2} for TRO. This makes up ~15% of the total (self + foreign) continuum absorption and 0.5% of the total water vapour absorption in this spectral region in the MLS case; this contribution will be greater for more humid atmospheres, and lesser for less humid ones. In most radiation models, the continuum at these wavelengths is parameterised using versions of MT_CKD. The results in many studies were obtained on the basis of MT_CKD-2.5 in the shortwave (e.g. [54]). Here, we use MT_CKD-3.2 as a benchmark, as this is the most recent version in which the water vapour continuum was updated.

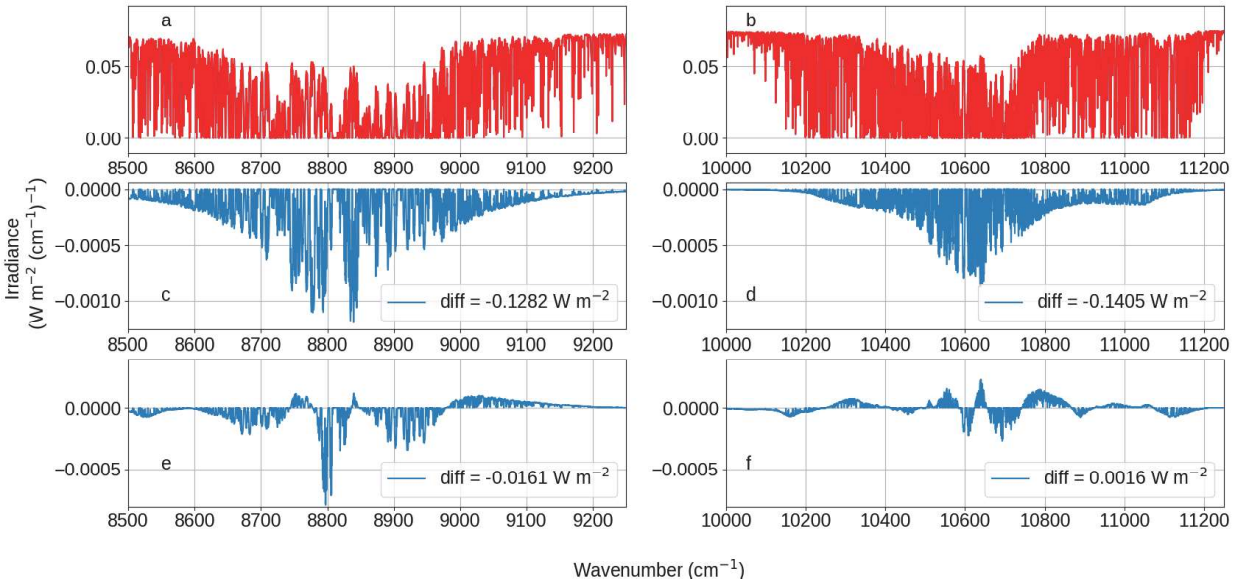

Fig. 11 Downwelling surface irradiance in the 8000-9250 cm^{-1} (panels a, c and e) and 10000-11200 cm^{-1} (panels b, d and f) bands for a mid-latitude summer atmosphere with overhead Sun (panels (a) and (b), the modelled impact of the MT_CKD-3.2 self-continuum in these spectral regions (panels (c) and (d)), and the change in surface irradiance from using the dimer-based model as opposed to MT_CKD-3.2 (panels (e) and (f)). A negative value in panels (c), (d), (e) and (f) indicates that the surface irradiance is being reduced, i.e. that additional absorption is occurring.

Figure 11 shows the calculated irradiances I at the surface for the model setup described above, with the MT_CKD-3.2 continuum shown in panels (a) and (b), the effect of the MT_CKD-3.2 self-continuum in this region (panels (c) and (d)), derived as $I_{\text{MT\_CKD}} - I_{\text{no self-continuum}}$ (where I_{MT_CKD} and $I_{no\ self\text{-}continuum}$ are the irradiances including the MT_CKD self-continuum and without it, respectively), and the effect of the change between the continuum obtained by extrapolating the dimer-based model in temperature and MT_CKD-3.2 in panels (e) and (f), derived as $I_{dimer\_model} - I_{\text{MT\_CKD}}$. The data in Fig. 11 was generated using MLS with an overhead Sun. The integrated difference (across the 8000-12000 cm^{-1} region) between the two in this case is relatively small (roughly 0.021 W m^{-2}), due to the broad similarity between the MT_CKD-3.2 and the effective water dimer spectra at the relevant temperatures. For the MLS case described in Fig. 11, the reduction in the surface irradiance across the two bands due to the self-continuum is 7% greater using the dimer-based model rather than MT_CKD-3.2; however, this is dominated by a decrease in irradiance of ~12.5% in the 8500-9250 cm^{-1} region, with a much smaller decrease (~1%) in irradiance in the 10000-11200 cm^{-1} region. A more detailed breakdown of the effect of the dimer-based model relative to MT_CKD-3.2 is presented in Table 4, for a range of atmospheric profiles and solar zenith angles. It is interesting to note that the increase in atmospheric absorption for the 60-degree solar zenith angle case in Table 4a using the dimer-based model is greater for the MLS atmosphere than the more humid TRO atmosphere in the 8500-9250 cm^{-1} band. This is an indication that the saturation of absorption lines in the tropical atmosphere reduces the effect of the enhanced continuum absorption at these higher

zenith angles. A saturation effect may also explain why the sign of the contribution changes in the 10000-11200 cm^{-1} band as the solar zenith angle increases in some cases.

The differences between MT_CKD-3.2 and the dimer-based model from this work are largest at the q-dimer band centres (according to blue curves in Fig. 9). These bands are included explicitly within our model, whereas in MT_CKD 3.2 they could be interpreted as being included indirectly in the "weak interaction term", which would spread their effect over a wider spectral range (see e.g. Fig. 10). It is clear from Fig. 11(e) that the narrow q-dimer peaks at ~8800 cm^{-1} have a significant impact on the total self-continuum absorption. There is better agreement with MT_CKD when integrating across the band, due in part due to the peaks and troughs in the dimer-based model cancelling each other out. The sign of the change relative to MT_CKD is dependent on the atmospheric conditions and solar zenith angle; it is likely that some of the spectral features are causing some bands to saturate sooner than others, within certain monomer band centres (which correspond to the q-dimer peaks which give the dimer-based model its more detailed spectral structure). Despite this, the presence of these peaks means that there may therefore be some useful spectral information that could be used to validate the dimer model. An atmospheric measurement with a high enough precision (e.g. those used as part of the Total Carbon Column Observing Network [55]) could potentially observe the sharply-peaked features especially noticeable, for example, at ~ 8530 and 10160 cm^{-1} (see Fig. 11).

While a change in the continuum may have an effect on water vapour retrievals (e.g. MODIS retrievals in the 915-965 nm band [56]), the significant cancellation of the peaks in this band (see e.g. Fig.11 c) results in a minimal change in the optical depth averaged over this spectral region going from MT_CKD-3.2 to the dimer-based model.

Table 4 Differences between the spectrally integrated surface irradiances (dimer-based model – MT_CKD-3.2) for different solar zenith angles and atmospheres, separated by spectral band.

a) 8500-9250 cm^{-1}

Solar zenith angle	TRO	MLS	SAW
0	-0.0218 (-11.7%)	-0.0161 (-12.5%)	-0.001 (-13.9%)
30	-0.0168 (-10.11%)	-0.0165 (-14.3%)	-0.0009 (-12.8%)
60	-0.0035 (-3.49%)	-0.0057 (-3.95%)	-0.0007 (-11.9%)

b) 10000-11200 cm^{-1}

Solar zenith angle	TRO	MLS	SAW
0	-0.0003 (-0.14%)	0.0016 (1.14%)	0.0002 (3.1%)
30	0.0002 (0.1%)	-0.0016 (-1.23%)	0.0002 (3.2%)
60	0.0011 (0.8%)	-0.0002 (-0.11%)	0.0002 (3.3%)

* Values are in W m^{-2} integrated over each band. Values in brackets indicate the percentage change in the surface irradiance due to self-continuum absorption within each band using the dimer-based model rather than MT_CKD-3.2. A negative number indicates that the surface irradiance has decreased (i.e. absorption has increased) when making this change from MT_CKD3.2 to the dimer-based model, and vice versa.

8 Conclusions

Measurements of IR radiation absorption in pure water vapour using Fourier transform spectroscopy were used to retrieve the water vapour self-continuum absorption in the 8800 and 10600 cm^{-1} water vapour bands at 398 and 431 K, and at pressures between 1000 and 4155 mbar. To our knowledge these are the first experimental derivations of the self-continuum in these bands. The dimer-based model of the water vapour self-continuum absorption, proposed for other infrared absorption bands in the earlier work [24], was parameterized and extended to higher wavenumbers

and higher temperatures by fitting the model to the experimental continuum spectra. A good quantitative description of the continuum absorption by this model was established, but required more water q-dimers than can be objectively explained by independent thermodynamic estimates. The MT_CKD-3.2 model demonstrates an underestimation of the observed continuum by about a factor of 1.5-2 on average in the measured absorption bands at elevated temperatures. Moreover, the characteristic spectral peaks observed in the measured self-continuum spectra are absent in MT_CKD-3.2. The temperature dependence of the total *effective* dimerization constant was derived in a broad temperature region from 268 to 430 K based on fitting of the dimer model to the measured continuum spectra with one fitted parameter (the equilibrium constant of quasibound dimers) in this work and the results of the lower temperature data in near-IR bands [24]. Using this temperature dependence, the dimer-based model for 8800 and 10600 cm^{-1} water vapour bands was then extrapolated from 400-430 K to the temperatures 260-296 K, and was found to be in reasonable agreement with the MT_CKD-3.2 continuum model at these temperatures (see Section 7), but with less agreement toward the band edges, and with some significant differences in narrow spectral regions (corresponding to absorption features of the quasibound dimer). The dimer-based model provides some support for the values produced by the MT_CKD model at atmospheric temperatures but not for the physical assumptions underlying that model. We suggest that the dimer-based model could now be considered as a replacement to MT_CKD for the in-band self-continuum as it is has now been shown to simulate, with reasonable accuracy, the observed self-continuum in several near-IR bands.

It is shown that without our empirical adjustment to the equilibrium constant of quasibound dimers, water dimers could account for not more than 50% of the detected water vapour self-continuum absorption within the 8800 and 10600 cm^{-1} absorption bands at the investigated temperatures. Possible reasons for the difference between this and the observed absorption could be the presence of additional mechanisms that contribute to the in-band continuum (such as intermediate line wings) or so-far neglected contributions in theoretical models of the bound dimer spectrum. In addition, to minimize the uncertainty of the water dimer model, the spectrum of quasibound dimers also needs to be studied in more detail. Hence, to advance understanding, improvements in theoretical calculations are needed. Measurements of the continuum strength over a wider range of experimental conditions would also be very beneficial in constraining theoretical models. The extension of such work to include the foreign continuum would also be beneficial.

Acknowledgments

Experimental part of the work was performed under financial support from the NERC-EPSRC (UK) funded consortium CAVIAR (Continuum Absorption at Visible and Infrared wavelengths and its Atmospheric Relevance (NE/D012082/1)). Processing of the experimental data and analysis was supported by the Russian Foundation for Basic Research (project number 19-32-90157\19) and the Ministry of Science and Higher Education of the Russian Federation (Program of the Basic Scientific Investigations, budget funds for V.E. Zuev Institute of Atmospheric Optics of Siberian Branch of the Russian Academy of Sciences). JE and KPS acknowledge support from the NERC "Advanced Spectroscopy for improved characterisation of the near-Infrared water vapour Continuum (ASPIC)" research grant (NE/R009848/1) during the writing phase of this paper. We thank the reviewers for many important suggestions.

References

[1] Hettner G. Über das ultrarote Absorptionsspektrum des Wasserdampfes. Ann Phys 1918;360:476–96. https://doi.org/https://doi.org/10.1002/andp.19183600603.

[2] Rädel G, Shine KP, Ptashnik I V. Global radiative and climate effect of the water vapour continuum at visible and near-infrared wavelengths. Q J R Meteorol Soc 2015;141:727–38. https://doi.org/10.1002/qj.2385.

[3] Shine KP, Ptashnik I V., Rädel G. The Water Vapour Continuum: Brief History and Recent Developments. Surv Geophys 2012;33:535–55. https://doi.org/10.1007/s10712-011-9170-y.

[4] Ptashnik I, Smith K, Shine K, Newnham D. Laboratory measurements of water vapour continuum absorption in spectral region 5000 – 5600 cm-1: Evidence for water dimers. Q J R Meteorol Soc 2004;130:2391–2408. https://doi.org/10.1256/qj.03.178.

[5] Ptashnik I V. Water dimers: an “ unknown " experiment. Atmos Ocean Opt 2005;18:324–6.

[6] Schofield DP, Kjaergaard HG. Calculated OH-stretching and HOH-bending vibrational transitions in the water dimer. Phys Chem Chem Phys 2003;5:3100–5. https://doi.org/10.1039/b304952c.

[7] Paynter D, Ptashnik I, Shine K, Smith K. Pure water vapour continuum measurements between 3100 and 4400 cm-1: evidence for water dimer absorption in near atmospheric conditions. Geoph Res Lett 2007;34:L12808. https://doi.org/10.1029/2007GL029259.

[8] Ptashnik IV. Evidence for the contribution of water dimers to the near-IR water vapour self-continuum. J Quant Spectrosc Radiat Transf 2008;109:831–852. https://doi.org/10.1016/j.jqsrt.2007.09.004.

[9] Ptashnik I, Shine KP, Vigasin AA. Water vapour self-continuum and water dimers : 1.Analysis of recent work. J Quant Spectrosc Radiat Transf 2011;112:1286–303. https://doi.org/10.1016/j.jqsrt.2011.01.012.

[10] Elsasser WM. Far infrared absorption of atmospheric water vapor. Astrophys J 1938;87:497–507. https://doi.org/10.1086/143940.

[11] Elsasser WM. Note on atmospheric absorption caused by the rotational water band. Phys Rev Journals 1938;53:768. https://doi.org/10.1103/PhysRev.53.768.

[12] Tvorogov SD, Nesmelova LI. Radiation processes in band wings of atmospheric gases. Izv Ros Akad Nauk SSSR, Fiz Atmos Okeana 1976;12:627–633.

[13] Tipping RH, Ma Q. Theory of the water vapor continuum and validations. Atmos Res 1995;36:69–94. https://doi.org/10.1016/0169-8095(94)00028-C.

[14] Ma Q, Tipping R, Leforestier C. Temperature dependences of mechanisms responsible for the water-vapor continuum absorption. I. Far wings of allowed lines. J Chem Phys 2008;128:124313. https://doi.org/10.1063/1.2839604.

[15] Klimeshina TE, Rodimova OB. Temperature dependence of the water vapor continuum absorption in the 3–5 μm spectral region. J Quant Spectrosc Radiat Transf 2013;119:77–83. https://doi.org/10.1016/j.jqsrt.2012.12.020.

[16] Viktorova AA, Zhevakin SA. Absorption of micro-radiowaves in air by water vapor dimers. Rep Acad Sci USSR 1966;171:1061–1064.

[17] Penner SS, Varanasi P. Spectral absorption coefficient in the pure rotational spectrum of water vapor. J Quant Spectr Radiat Transf 1967;7:687–90. https://doi.org/10.1016/0022-4073(67)90024-6.

[18] Vigasin AA. Bound, metastable and free states of bimolecular complexes. Infrared Phys 1991;32:451–70. https://doi.org/10.1016/0020-0891(91)90135-3.

[19] Vigasin AA. Bimolecular absorption in atmospheric gases. Weakly Interact. Mol. Pairs Unconv. Absorbers Radiat. Atmos., Kluwer Academic Publishers; 2003, p. 23–48. https://doi.org/10.1007/978-94-010-0025-3_2.

[20] Ptashnik I V, Smith KM, Shine KP, Newnham DA. Laboratory measurements of water vapour continuum absorption in spectral region 5000 – 5600 cm − 1 : Evidence for water dimers. Q J R Meteorol Soc 2004;130:2391–408. https://doi.org/10.1256/qj.03.178.

[21] Vigasin AA. On the possibility to quantify contributions from true bound and metastable pairs to infrared absorption in pressurised water vapour. Mol Phys 2010;108:2309–13.

https://doi.org/10.1080/00268971003781563.
[22] Ma Q, Tipping RH, Leforestier C. Temperature dependences of mechanisms responsible for the water-vapor continuum absorption. I. Far wings of allowed lines. J Chem Phys 2008;128:124313. https://doi.org/https://doi.org/10.1063/1.2839604.
[23] Rodimova OB. Carbon Dioxide and Water Vapor Continuum Absorption in the Infrared Spectral Region. Atmos Ocean Opt 2018;31:564–9. https://doi.org/10.1134/S1024856018060143.
[24] Ptashnik I V., Klimeshina TE, Solodov AA, Vigasin AA. Spectral composition of the water vapour self-continuum absorption within 2.7 and 6.25 μm bands. J Quant Spectrosc Radiat Transf 2019;228:97–105. https://doi.org/10.1016/j.jqsrt.2019.02.024.
[25] Vaida V, Daniel JS, Kjaergaard HG, Goss LM, Tuck AF. Atmospheric absorption of near infrared and visible solar radiation by the hydrogen bonded water dimer. Q J R Meteorol Soc 2001;127:1627–43. https://doi.org/10.1002/qj.49712757509.
[26] Daniel JS, Solomon S, Kjaergaard HG, Schofield DP. Atmospheric water vapor complexes and the continuum. Geophys Res Lett 2004;31:L06118(1-4). https://doi.org/10.1029/2003gl018914.
[27] Scribano Y, Leforestier C. Contribution of water dimer absorption to the millimeter and far infrared atmospheric water continuum. J Chem Phys 2007;126:1–12. https://doi.org/10.1063/1.2746038.
[28] Kjaergaard HG, Garden AL, Chaban GM, Gerber RB, Matthews DA, Stanton JF. Calculation of vibrational transition frequencies and intensities in water dimer: Comparison of different vibrational approaches. J Phys Chem A 2008;112:4324–35. https://doi.org/10.1021/jp710066f.
[29] Salmi T, Hänninen V, Garden AL, Kjaergaard HG, Tennyson J, Halonen L. Calculation of the O - H stretching vibrational overtone spectrum of the water dimer. J Phys Chem A 2008;112:6305–12. https://doi.org/10.1021/jp800754y.
[30] Tretyakov MY, Serov EA, Koshelev MA, Parshin V V., Krupnov AF. Water dimer rotationally resolved millimeter-wave spectrum observation at room temperature. Phys Rev Lett 2013;110:093001(1-4). https://doi.org/10.1103/PhysRevLett.110.093001.
[31] Serov EA, Koshelev MA, Odintsova TA, Parshin V V., Tretyakov MY. Rotationally resolved water dimer spectra in atmospheric air and pure water vapour in the 188-258 GHz range. Phys Chem Chem Phys 2014;16:26221–33. https://doi.org/10.1039/c4cp03252g.
[32] Ptashnik I V. Water vapour continuum absorption: Short prehistory and current status. Opt Atmos i Okeana 2015;28:443–59. https://doi.org/10.15372/AOO20150508.
[33] Mlawer EJ, Payne VH, Moncet JL, Delamere JS, Alvarado MJ, Tobin DC. Development and recent evaluation of the MT-CKD model of continuum absorption. Philos Trans R Soc A Math Phys Eng Sci 2012;370:2520–56. https://doi.org/10.1098/rsta.2011.0295.
[34] Mitsel' AA, Ptashnik I V., Firsov KM, Fomin BA. Efficient technique for line-by-line calculating the transmittance of the absorbing atmosphere. Atmos Ocean Opt 1995;8:1547–51. https://doi.org/10.1016/0022-4073(95)00029-K.
[35] Gordon IE, Rothman LS, Hill C, Kochanov R V, Tan Y, Bernath PF, et al. The HITRAN2016 molecular spectroscopic database. J Quant Spectrosc Radiat Transf 2017;203:3–69. https://doi.org/10.1016/j.jqsrt.2017.06.038.
[36] Mondelain D, Aradj A, Kassi S, Campargue A. The water vapour self-continuum by CRDS at room temperature in the 1.6 μm transparency window. J Quant Spectrosc Radiat Transf 2013;130:381–91. https://doi.org/10.1016/j.jqsrt.2013.07.006.
[37] Ponomarev YN, Ptashnik I V., Solodov AA, Solodov AM. Main sources of uncertainties in measuring weak near-infrared water vapor continuum absorption with a Fourier spectrometer with a long optical path. Atmos Ocean Opt 2017;30:481–4. https://doi.org/10.1134/S1024856017050098.
[38] Simonova AA, Ptashnik IV. Contribution of errors in line parameters to the retrieval of the vapor continuum absorption within 0.94- and 1.13-μm bands. Atmos Ocean Opt 2019;32:375–7. https://doi.org/10.1134/S1024856019040146.
[39] Serov EA, Odintsova TA, Tretyakov MY, Semenov VE. On the origin of the water vapor continuum absorption within rotational and fundamental vibrational bands. J Quant Spectrosc

Radiat Transf 2017;193:1–12. https://doi.org/10.1016/j.jqsrt.2017.02.011.
[40] Scribano Y, Goldman N, Saykally RJ, Leforestier C. Water Dimers in the Atmosphere III : Equilibrium Constant from a Flexible Potential. J Phys Chem A 2006;110:5411–9. https://doi.org/10.1021/jp056759k.
[41] Buryak I, Vigasin AA. Classical calculation of the equilibrium constants for true bound dimers using complete potential energy surface. J Chem Phys 2015;143:234304(1-8). https://doi.org/10.1063/1.4938050.
[42] Kuyanov-Prozument K, Choi MY, Vilesov AF. Spectrum and infrared intensities of OH-stretching bands of water dimers. J Chem Phys 2010;132:014304(1-7). https://doi.org/10.1063/1.3276459.
[43] Birk M, Wagner G, Loos J, Shine KP. 3 μm Water vapor self- and foreign-continuum: New method for determination and new insights into the self-continuum. J Quant Spectrosc Radiat Transf 2020;253:107134. https://doi.org/10.1016/j.jqsrt.2020.107134.
[44] Rocher-Casterline B, Ch'ng L, Mollner A, Reisler H. Communication: determination of the bond dissociation energy (D0) of the water dimer, (H2O)2, by velocity map imaging. J Chem Phys 2011;134:211101(1-4). https://doi.org/10.1063/1.3598339.
[45] Tretyakov MY, Serov EA, Odintsova TA. Equilibrium thermodynamic state of water vapor and the collisional interaction of molecules. Radiophys Quantum Electron 2012;54:700–16. https://doi.org/10.1007/s11141-012-9332-x.
[46] Leforestier C. Water dimer equilibrium constant calculation: A quantum formulation including metastable states. J Chem Phys 2014;140:074106. https://doi.org/10.1063/1.4865339.
[47] Ruscic B. Active thermochemical tables: Water and water dimer. J Phys Chem A 2013;117:11940–53. https://doi.org/10.1021/jp403197t.
[48] Mackeprang K, Kjaergaard HG, Salmi T, Hänninen V, Halonen L. The effect of large amplitude motions on the transition frequency redshift in hydrogen bonded complexes: A physical picture. J Chem Phys 2014;140:184309(1-9). https://doi.org/10.1063/1.4873420.
[49] Mackeprang K, Hänninen V, Halonen L, Kjaergaard HG. The effect of large amplitude motions on the vibrational intensities in hydrogen bonded complexes. J Chem Phys 2015;142:094304(1-10). https://doi.org/10.1063/1.4913737.
[50] Collins WD, Ramaswamy V, Schwarzkopf MD, Sun Y, Portmann RW, Fu Q, et al. Radiative forcing by well-mixed greenhouse gases : Estimates from climate models in the Intergovernmental Panel on Climate Change (IPCC) Fourth Assessment Report (AR4). J Geophys Res 2006;111:D14317(1-15). https://doi.org/10.1029/2005JD006713.
[51] Dudhia A. The Reference Forward Model (RFM). J Quant Spectrosc Radiat Transf 2017;186:243–53. https://doi.org/10.1016/j.jqsrt.2016.06.018.
[52] Stamnes K, Tsay S, Wiscombe W, Jayaweera K. Numerically stable algorithm for discrete-ordinate-method radiative transfer in multiple scattering and emitting layered media. Appl Opt 1988;27:2502–9. https://doi.org/https://doi.org/10.1364/AO.27.002502.
[53] Kurucz RL, Bell B. Atomic Line Data. Kurucz CD-ROM No 23, Cambridge, Smithson Astrophys Obs 1995.
[54] Paynter DJ, Ramaswamy V. An assessment of recent water vapor continuum measurements upon longwave and shortwave radiative transfer. J Geophys Res 2011;116:D20302(1-13). https://doi.org/10.1029/2010JD015505.
[55] Wunch D, Toon GC, Blavier JFL, Washenfelder RA, Notholt J, Connor BJ, et al. The total carbon column observing network. Philos Trans R Soc A 2011;369:2087–112. https://doi.org/10.1098/rsta.2010.0240.
[56] Gao B-C, Kaufman YJ. Water vapor retrievals using Moderate Resolution Imaging Spectroradiometer (MODIS) near-infrared channels. J Geophys Res Atmos 2003;108:1–10. https://doi.org/10.1029/2002jd003023.

Appendix

Table 1. Cross-section absorption, $C_s(\nu)$ [$cm^2 molec^{-1} atm^{-1}$], of water vapour self-continuum experimentally retrieved in this work at 398 and 431 K within 8800 and 10600 cm^{-1} absorption bands.

398 K						431 K					
ν, cm^{-1}	$C_s(\nu)$	$C^{err}_s(\nu)$	ν, cm^{-1}	$C_s(\nu)$	$C^{err}_s(\nu)$	ν, cm^{-1}	$C_s(\nu)$	$C^{err}_s(\nu)$	ν, cm^{-1}	$C_s(\nu)$	$C^{err}_s(\nu)$
8502.76	6.85E-25	8.23E-26	10135.45	1.04E-25	2.62E-26	8531.26	3.9E-25	8.61E-26	10052.73	2.41E-26	3.01E-27
8503.12	6.73E-25	8.19E-26	10136.23	8.55E-26	3.19E-26	8535.51	4.57E-25	7.71E-26	10094.07	3.74E-26	7.38E-27
8503.18	6.84E-25	8.23E-26	10158.86	1.83E-25	3.70E-26	8548.44	5.00E-25	8.92E-26	10136.20	8.61E-26	1.06E-26
8510.23	7.16E-25	1.25E-25	10165.49	1.97E-25	5.53E-26	8566.64	6.90E-25	1.42E-25	10140.36	6.48E-26	1.51E-26
8512.94	6.43E-25	1.30E-25	10165.88	1.91E-25	5.63E-26	8573.81	5.89E-25	1.80E-25	10160.61	1.33E-25	2.81E-26
8513.09	6.40E-25	1.30E-25	10171.94	2.05E-25	5.72E-26	8586.10	7.64E-25	1.52E-25	10162.35	1.59E-25	2.86E-26
8531.32	7.85E-25	1.66E-25	10180.58	1.94E-25	5.81E-26	8598.40	1.09E-24	1.36E-25	10166.23	1.17E-25	4.08E-26
8531.69	7.75E-25	1.65E-25	10189.74	2.19E-25	4.83E-26	8612.80	1.26E-24	2.58E-25	10189.83	1.33E-25	2.64E-26
8535.36	7.42E-25	1.44E-25	10193.60	2.47E-25	4.69E-26	8624.98	1.51E-24	3.64E-25	10193.45	1.50E-25	2.28E-26
8535.51	7.36E-25	1.44E-25	10204.45	3.20E-25	6.90E-26	8633.68	1.90E-24	3.70E-25	10232.14	2.74E-25	2.80E-26
8535.60	7.32E-25	1.45E-25	10232.14	4.15E-25	5.68E-26	8643.08	2.24E-24	3.17E-25	10256.85	3.21E-25	5.20E-26
8537.83	8.53E-25	1.80E-25	10256.82	6.04E-25	1.00E-25	8643.17	2.24E-24	3.17E-25	10286.62	2.59E-25	3.37E-26
8541.11	5.89E-25	1.64E-25	10263.09	4.88E-25	9.67E-26	8643.30	2.25E-24	3.16E-25	10286.77	2.58E-25	5.29E-26
8546.57	8.81E-25	1.52E-25	10286.65	4.23E-25	5.84E-26	8656.13	2.71E-24	4.71E-25	10302.29	2.68E-25	3.62E-26
8548.44	7.99E-25	1.45E-25	10294.42	4.62E-25	8.09E-26	8671.47	2.84E-24	5.23E-25	10333.50	4.63E-25	4.14E-26
8548.68	8.21E-25	1.46E-25	10299.28	4.70E-25	5.95E-26	8683.28	3.51E-24	5.42E-25	10334.02	4.55E-25	7.39E-26
8553.83	7.20E-25	2.01E-25	10302.29	4.13E-25	7.27E-26	8690.75	3.61E-24	5.18E-25	10378.85	8.37E-25	1.54E-25
8565.37	1.12E-24	2.43E-25	10302.47	4.17E-25	7.23E-26	8701.60	3.53E-24	4.79E-25	10379.13	8.74E-25	9.39E-26
8573.87	1.10E-24	3.27E-25	10322.60	5.81E-25	7.98E-26	8701.66	3.53E-24	4.78E-25	10400.43	1.03E-24	2.00E-25
8585.92	1.03E-24	2.26E-25	10333.78	7.29E-25	7.12E-26	8708.95	3.48E-24	3.86E-25	10441.20	1.91E-24	1.69E-25
8586.07	1.22E-24	2.48E-25	10333.93	7.22E-25	7.52E-26	8727.97	3.29E-24	3.67E-25	10442.34	1.82E-24	2.92E-25
8598.37	1.72E-24	2.39E-25	10334.14	7.53E-25	1.14E-25	8745.99	3.10E-24	3.49E-25	10457.05	1.82E-24	3.59E-25
8598.85	1.70E-24	2.30E-25	10350.62	7.37E-25	1.53E-25	8752.80	3.02E-24	3.14E-25	10470.67	1.93E-24	4.29E-25
8607.14	1.45E-24	4.44E-25	10359.54	1.03E-24	2.10E-25	8768.43	3.35E-24	3.71E-25	10480.01	2.20E-24	2.84E-25
8626.03	3.83E-24	8.44E-25	10378.92	1.40E-24	2.27E-25	8769.37	3.37E-24	3.71E-25	10487.24	1.90E-24	2.43E-25
8630.64	4.31E-24	9.40E-25	10379.28	1.38E-24	1.49E-25	8779.55	3.52E-24	3.57E-25	10494.26	2.06E-24	3.72E-25
8633.74	4.37E-24	7.43E-25	10395.52	1.98E-24	3.90E-25	8787.75	3.14E-24	3.74E-25	10500.87	2.20E-24	3.63E-25
8643.17	4.08E-24	6.79E-25	10400.64	1.95E-24	3.24E-25	8794.05	4.11E-24	4.10E-25	10512.73	2.13E-24	1.83E-25
8656.13	5.16E-24	1.01E-24	10431.01	2.53E-24	4.05E-25	8794.59	4.04E-24	4.06E-25	10581.00	2.40E-24	2.92E-25
8669.69	5.71E-24	1.02E-24	10442.28	2.78E-24	2.62E-25	8843.98	3.81E-24	3.55E-25	10597.46	2.04E-24	2.84E-25
8671.41	5.98E-24	1.03E-24	10457.05	3.17E-24	3.82E-25	8859.34	4.51E-24	4.75E-25	10613.25	1.44E-24	2.27E-25
8683.28	7.30E-24	1.15E-24	10470.70	4.13E-24	5.58E-25	8873.02	5.15E-24	5.85E-25	10618.25	1.58E-24	2.11E-25
8690.87	7.15E-24	1.11E-24	10479.98	3.85E-24	4.83E-25	8891.16	5.75E-24	6.61E-25	10626.69	1.76E-24	2.21E-25
8690.96	7.17E-24	1.11E-24	10482.03	3.99E-24	5.41E-25	8894.84	5.50E-24	6.63E-25	10646.64	1.60E-24	2.65E-25
8701.66	6.72E-24	9.32E-25	10487.36	3.20E-24	4.07E-25	8902.76	4.83E-24	6.68E-25	10664.18	1.72E-24	4.87E-25
8708.17	6.44E-24	8.43E-25	10510.41	2.87E-24	4.61E-25	8921.35	4.14E-24	7.08E-25	10677.86	2.14E-24	3.83E-25
8724.71	6.49E-24	1.95E-24	10512.70	3.42E-24	3.31E-25	8945.07	3.55E-24	6.54E-25	10693.04	2.13E-24	4.68E-25
8735.68	7.67E-24	2.08E-24	10515.78	3.37E-24	4.67E-25	9049.21	3.16E-25	8.20E-26	10715.40	2.21E-24	4.17E-25
8741.22	6.05E-24	1.33E-24	10535.78	3.29E-24	3.57E-25	9059.81	2.81E-25	8.33E-26	10783.20	2.40E-25	8.05E-26
8746.11	5.74E-24	7.14E-25	10548.02	3.14E-24	5.98E-25	9078.25	1.81E-25	4.16E-26	10787.47	3.05E-25	1.04E-25
8746.23	5.64E-24	7.00E-25	10560.70	3.08E-24	6.50E-25	9089.46	1.70E-25	3.58E-26	10790.91	1.74E-25	6.28E-26
8752.80	5.34E-24	7.35E-25	10563.93	3.66E-24	5.54E-25	9096.82	1.81E-25	2.90E-26	10793.16	1.99E-25	8.58E-26
8756.80	5.27E-24	7.94E-25	10577.49	3.63E-24	5.35E-25	9116.82	1.80E-25	8.79E-27	10800.80	1.71E-25	4.79E-26
8757.98	5.43E-24	7.96E-25	10581.58	4.37E-24	4.97E-25	9117.31	1.64E-25	9.11E-27	10810.32	1.81E-25	4.02E-26
8768.50	6.34E-24	8.62E-25	10596.56	3.83E-24	5.50E-25	9127.97	1.38E-25	1.38E-26	10823.88	2.07E-25	5.04E-26
8769.37	6.31E-24	8.49E-25	10613.37	2.90E-24	4.29E-25	9140.69	1.01E-25	1.30E-26	10834.48	2.03E-25	2.99E-26
8775.85	6.44E-24	7.58E-25	10618.80	2.95E-24	3.42E-25	9144.67	9.80E-26	1.18E-26	10863.29	2.70E-25	1.70E-26
8777.75	6.46E-24	7.01E-25	10626.63	3.35E-24	4.39E-25	9144.76	9.80E-26	1.18E-26	10879.62	2.67E-25	3.48E-26
8779.43	6.13E-24	7.47E-25	10629.16	2.87E-24	4.59E-25	9155.57	8.95E-26	8.79E-27	10907.28	3.50E-25	3.58E-26
8786.39	6.18E-24	8.85E-25	10634.38	2.53E-24	4.04E-25	9155.69	8.94E-26	8.76E-27	10928.86	3.90E-25	4.05E-26
8787.69	6.31E-24	9.13E-25	10646.70	2.85E-24	3.24E-25	9174.98	7.38E-26	6.91E-27	10931.45	3.62E-25	3.86E-26
8794.35	6.98E-24	8.02E-25	10652.76	3.00E-24	6.82E-25	9175.13	7.36E-26	6.90E-27	10935.61	3.61E-25	4.00E-26
8794.62	6.93E-24	7.97E-25	10662.67	3.27E-24	7.52E-25	9184.89	6.57E-26	6.42E-27	10938.62	3.48E-25	4.01E-26
8804.66	7.70E-24	8.51E-25	10664.04	3.46E-24	8.74E-25	9184.98	6.56E-26	6.42E-27	10958.75	3.64E-25	2.89E-26
8834.67	6.16E-24	7.42E-25	10665.20	3.90E-24	8.21E-25	9188.30	7.11E-26	6.73E-27	10969.54	2.99E-25	2.70E-26
8839.08	5.53E-24	7.33E-25	10677.92	4.25E-24	6.42E-25	9188.39	7.13E-26	6.74E-27	10982.80	2.73E-25	5.94E-26

8844.04	6.67E-24	8.32E-25	10693.10	4.22E-24	7.62E-25	9188.63	7.17E-26	6.77E-27	10989.60	2.50E-25	4.38E-26
8853.74	6.97E-24	1.56E-24	10715.76	4.47E-24	6.84E-25	9190.41	6.96E-26	6.74E-27	11006.60	2.48E-25	6.24E-26
8855.97	7.22E-24	1.73E-24	10800.83	2.71E-25	7.81E-26	9194.60	5.77E-26	6.47E-27	11013.83	2.42E-25	4.61E-26
8859.31	7.24E-24	1.99E-24	10810.29	2.99E-25	6.79E-26	--	--	--	11039.87	1.90E-25	2.08E-26
8864.14	6.91E-24	2.21E-24	10817.76	3.04E-25	6.70E-26	--	--	--	11047.10	2.03E-25	1.66E-26
8873.08	1.02E-23	1.41E-24	10823.37	3.72E-25	6.28E-26	--	--	--	11052.52	1.90E-25	1.53E-26
8875.86	1.06E-23	1.62E-24	10834.88	2.80E-25	5.50E-26	--	--	--	11062.83	1.96E-25	1.17E-26
8889.36	1.20E-23	1.62E-24	10835.12	2.83E-25	5.87E-26	--	--	--	11067.05	1.96E-25	3.00E-26
8891.19	1.13E-23	1.50E-24	10835.24	2.86E-25	4.63E-26	--	--	--	11083.38	2.15E-25	4.30E-26
8894.93	1.17E-23	1.82E-24	10839.34	2.84E-25	5.44E-26	--	--	--	11112.60	3.60E-25	3.53E-26
8902.79	1.03E-23	1.92E-24	10863.17	3.50E-25	5.22E-26	--	--	--	--	--	--
8920.39	8.52E-24	1.57E-24	10863.32	3.58E-25	4.86E-26	--	--	--	--	--	--
8921.33	8.55E-24	1.53E-24	10863.41	3.60E-25	4.81E-26	--	--	--	--	--	--
8930.79	6.93E-24	1.4E-24	10863.56	3.62E-25	4.77E-26	--	--	--	--	--	--
8943.62	7.52E-24	1.27E-24	10866.46	4.04E-25	5.76E-26	--	--	--	--	--	--
8945.13	7.07E-24	1.25E-24	10866.54	4.02E-25	5.76E-26	--	--	--	--	--	--
8970.98	2.36E-24	8.46E-25	10868.78	3.92E-25	5.05E-26	--	--	--	--	--	--
8972.73	2.74E-24	6.18E-25	10879.56	3.97E-25	7.11E-26	--	--	--	--	--	--
8994.16	1.98E-24	4.21E-25	10879.71	4.01E-25	6.72E-26	--	--	--	--	--	--
9034.03	7.70E-25	7.21E-26	10890.14	4.31E-25	8.25E-26	--	--	--	--	--	--
9048.94	5.58E-25	6.98E-26	10907.19	5.45E-25	8.03E-26	--	--	--	--	--	--
9059.32	5.07E-25	6.29E-26	10928.89	5.87E-25	9.68E-26	--	--	--	--	--	--
9078.25	2.92E-25	4.91E-26	10931.60	5.91E-25	8.85E-26	--	--	--	--	--	--
9078.68	3.25E-25	4.52E-26	10935.61	5.90E-25	8.57E-26	--	--	--	--	--	--
9087.96	3.66E-25	6.55E-26	10938.86	6.03E-25	8.71E-26	--	--	--	--	--	--
9089.58	3.16E-25	6.15E-26	10958.78	5.70E-25	6.23E-26	--	--	--	--	--	--
9096.85	2.95E-25	6.07E-26	10969.45	4.64E-25	5.59E-26	--	--	--	--	--	--
9104.57	3.15E-25	3.49E-26	10982.43	5.43E-25	8.06E-26	--	--	--	--	--	--
9116.75	2.33E-25	1.65E-26	10982.83	5.45E-25	7.58E-26	--	--	--	--	--	--
9127.94	2.01E-25	2.69E-26	10989.49	4.49E-25	8.82E-26	--	--	--	--	--	--
9128.00	2.01E-25	2.71E-26	11005.30	4.85E-25	8.77E-26	--	--	--	--	--	--
9137.65	1.90E-25	3.05E-26	11013.83	4.56E-25	8.02E-26	--	--	--	--	--	--
9144.27	2.07E-25	2.89E-26	11014.92	4.75E-25	9.05E-26	--	--	--	--	--	--
9144.49	2.21E-25	2.94E-26	11039.59	2.86E-25	3.94E-26	--	--	--	--	--	--
9144.70	2.13E-25	2.93E-26	11039.84	2.98E-25	3.81E-26	--	--	--	--	--	--
9155.65	1.62E-25	2.05E-26	11046.83	2.68E-25	4.53E-26	--	--	--	--	--	--
9156.55	1.64E-25	1.95E-26	11047.22	2.84E-25	4.60E-26	--	--	--	--	--	--
9159.71	1.58E-25	1.63E-26	11052.31	2.74E-25	2.43E-26	--	--	--	--	--	--
9162.87	1.29E-25	1.40E-26	11052.46	2.64E-25	2.80E-26	--	--	--	--	--	--
9165.45	1.3E-25	1.49E-26	11052.73	2.53E-25	3.05E-26	--	--	--	--	--	--
9166.14	1.38E-25	1.53E-26	11062.89	2.69E-25	3.69E-26	--	--	--	--	--	--
9175.04	1.10E-25	1.50E-26	11063.16	2.65E-25	3.76E-26	--	--	--	--	--	--
9175.40	1.14E-25	1.51E-26	11066.56	2.76E-25	4.37E-26	--	--	--	--	--	--
9188.51	9.91E-26	1.18E-26	11066.68	2.56E-25	3.77E-26	--	--	--	--	--	--
9188.69	9.56E-26	1.17E-26	11083.74	3.93E-25	7.52E-26	--	--	--	--	--	--
9188.93	9.62E-26	1.16E-26	11112.82	5.48E-25	6.26E-26	--	--	--	--	--	--
9189.14	1.01E-25	1.19E-26	--	--	--	--	--	--	--	--	--
9190.44	9.25E-26	1.20E-26	--	--	--	--	--	--	--	--	--
9190.59	9.18E-26	1.21E-26	--	--	--	--	--	--	--	--	--
9194.50	8.53E-26	1.34E-26	--	--	--	--	--	--	--	--	--
9196.16	1.02E-25	1.43E-26	--	--	--	--	--	--	--	--	--
9200.35	9.83E-26	1.67E-26	--	--	--	--	--	--	--	--	--

850

Figure 1

Click here to access/download;Figure;Fig.1.pdf

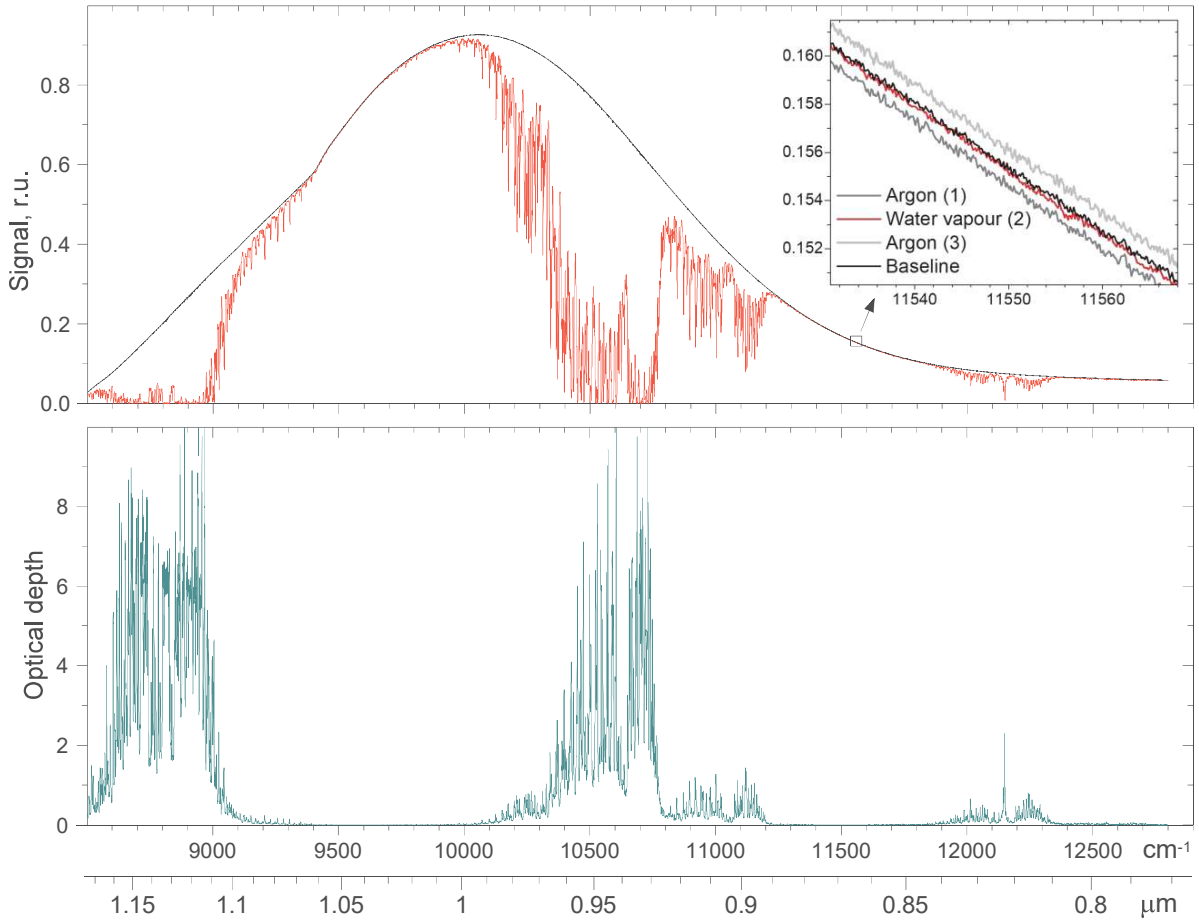

Figure 2

Click here to access/download;Figure;Fig.2.pdf

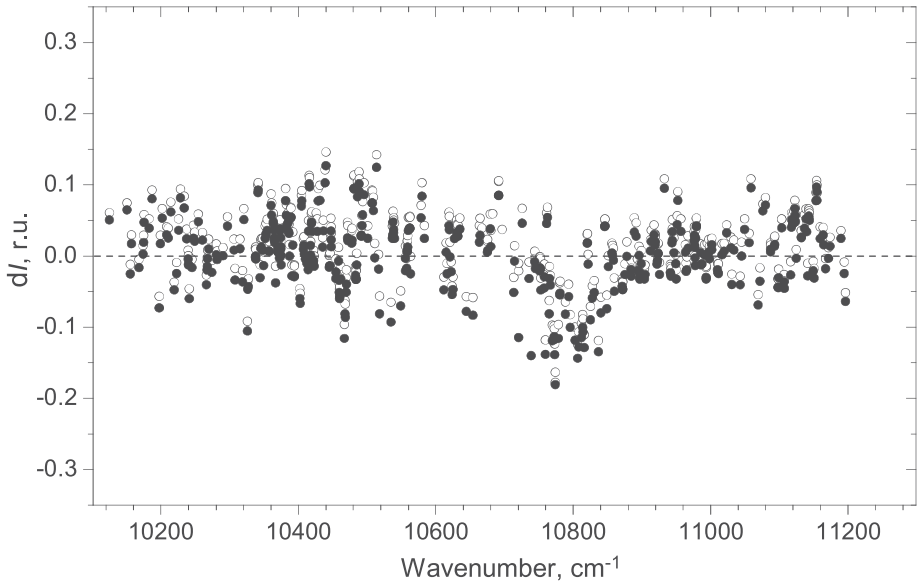

Figure 3

Click here to access/download;Figure;Fig.3.pdf

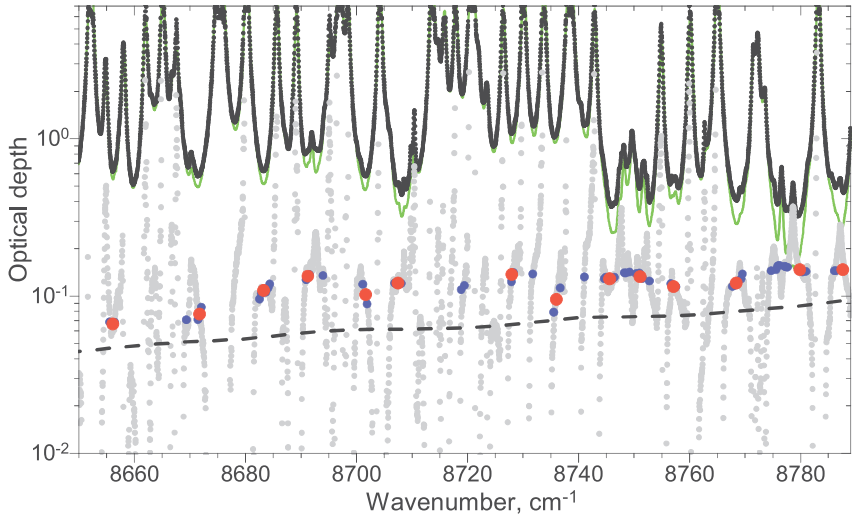

Figure 4

Click here to access/download;Figure;Fig.4.pdf

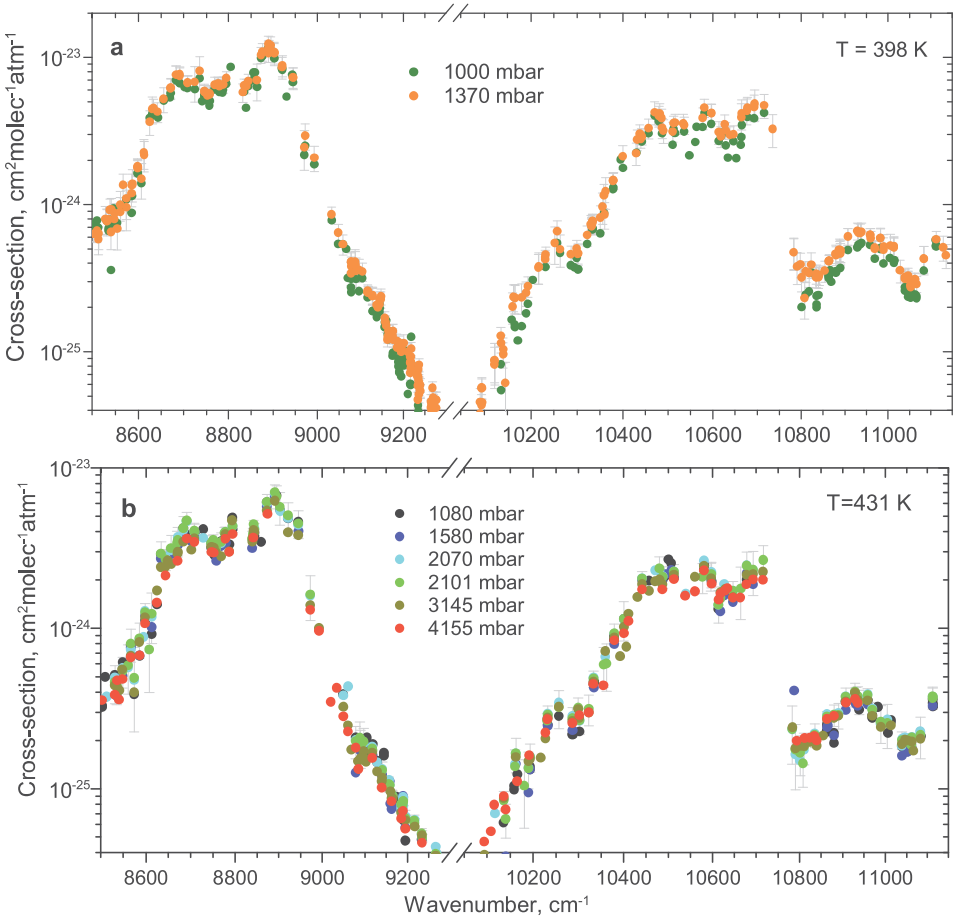

Figure 5

Click here to access/download;Figure;Fig.5.pdf

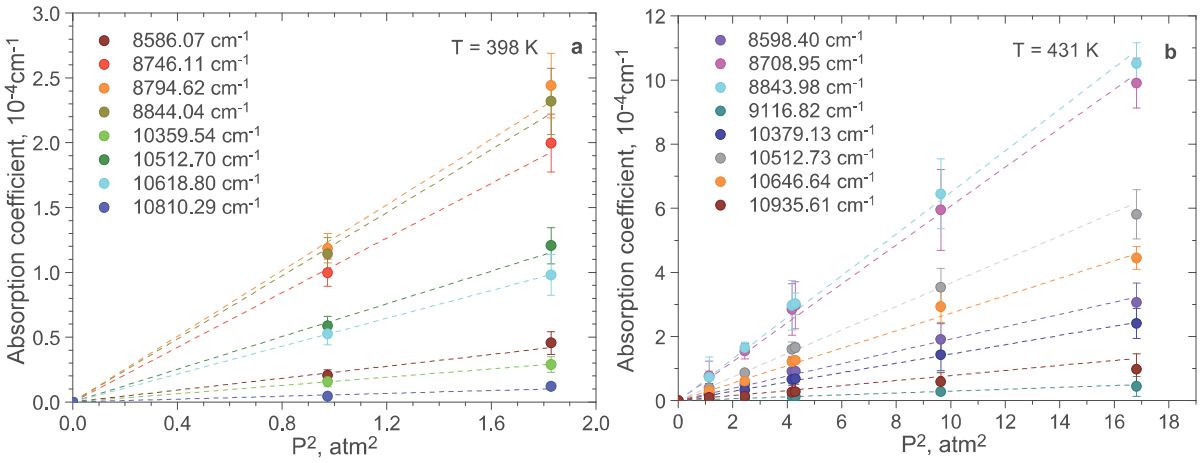

Figure 6

Click here to access/download;Figure;Fig.6.pdf

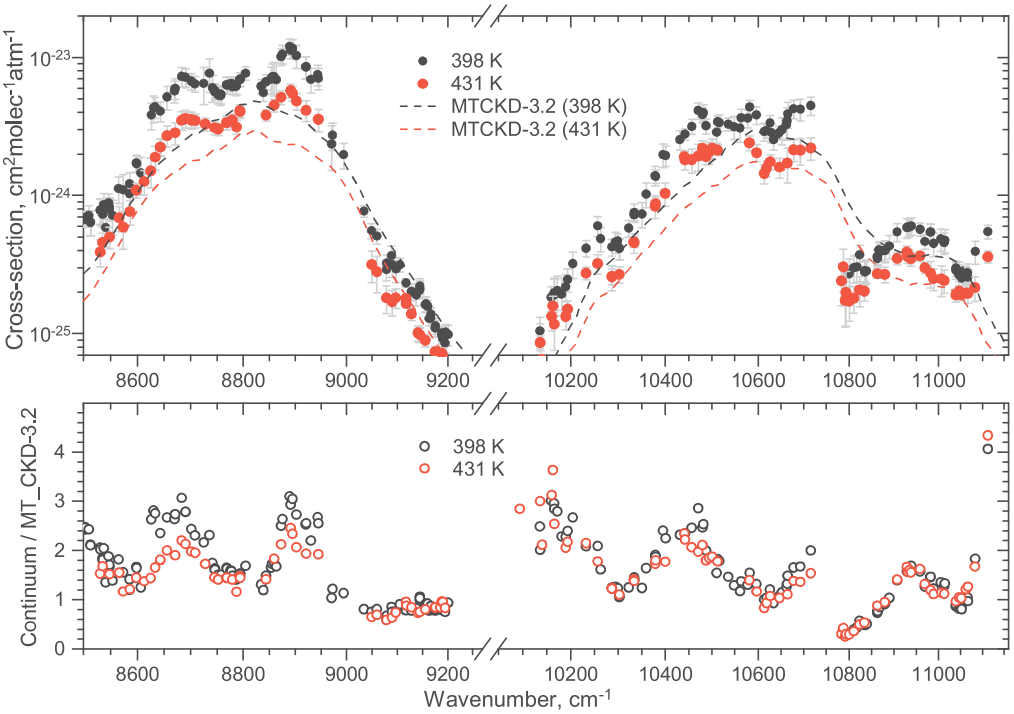

Figure 7

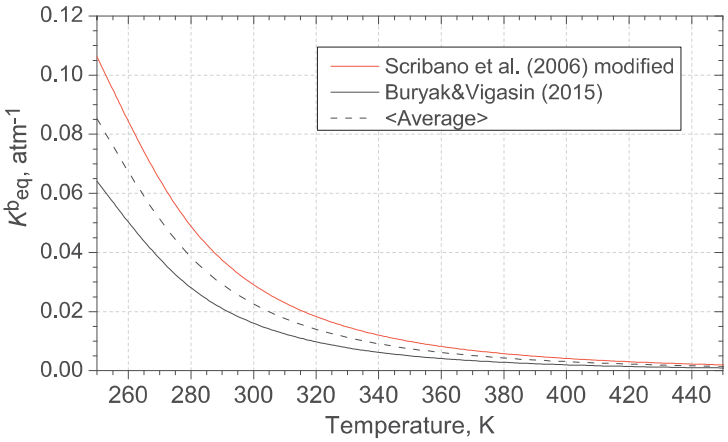

Figure 8

Click here to access/download;Figure;Fig.8.pdf

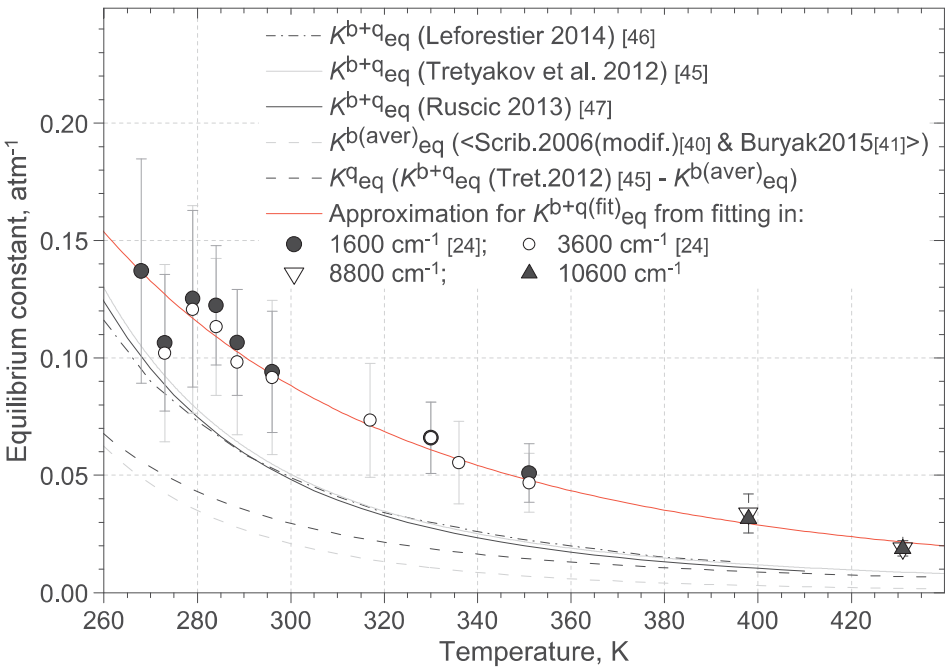

Figure 9 (a-f)

Click here to access/download;Figure;Fig.9(a-f).pdf

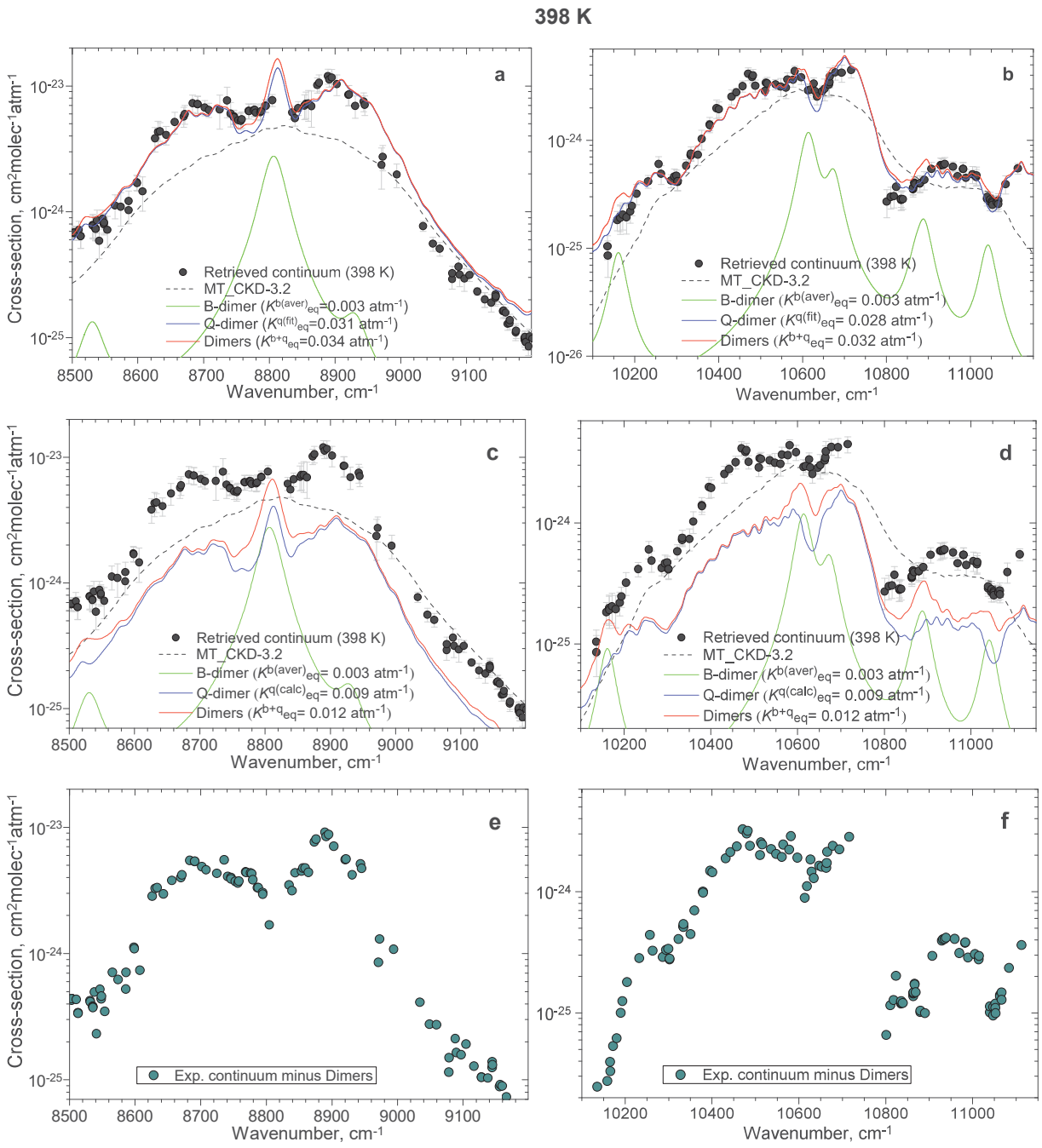

Figure 9 (j-l)

Click here to access/download;Figure;Fig.9(j-l).pdf

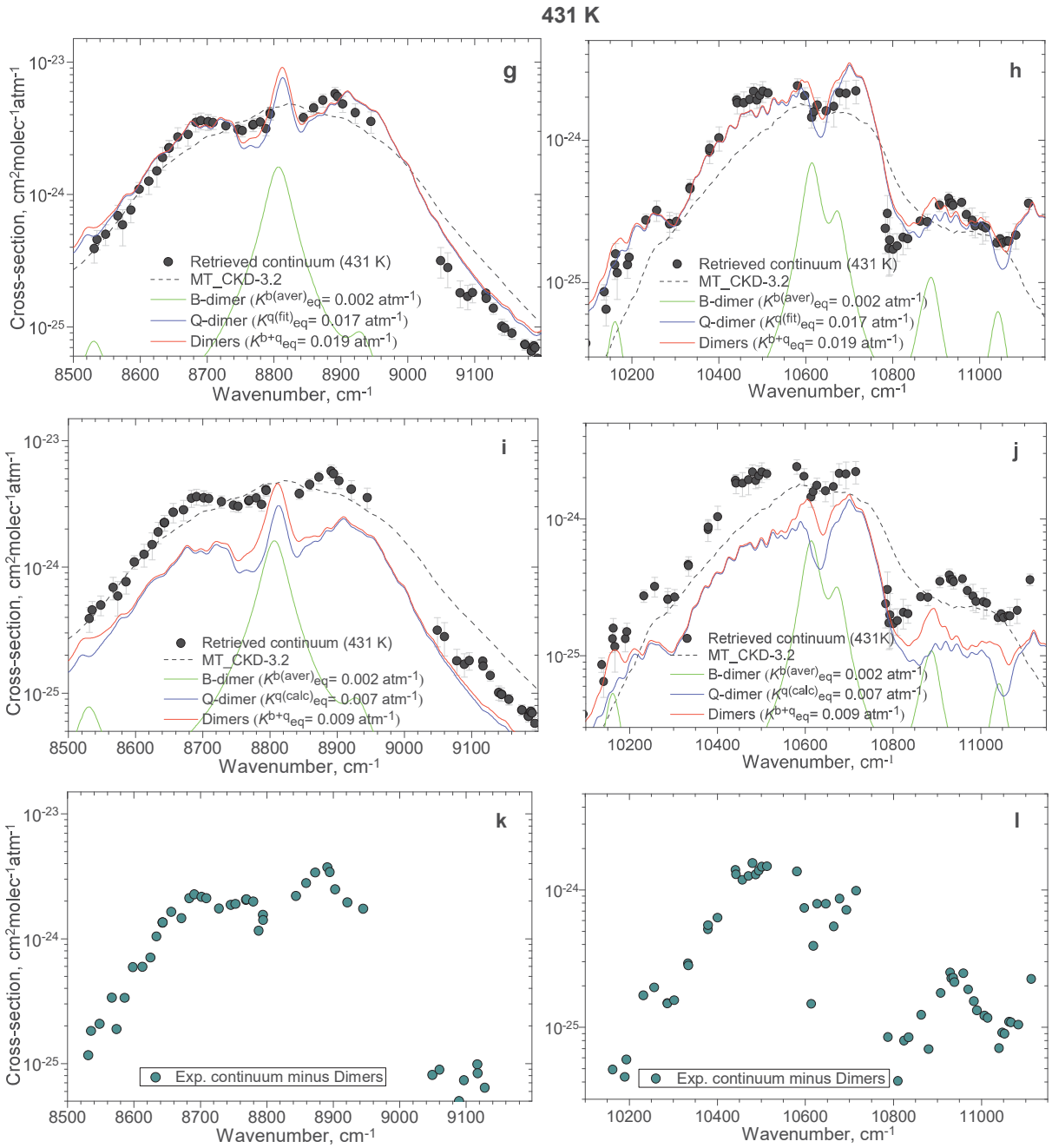

Figure 10

Click here to access/download;Figure;Fig.10.pdf

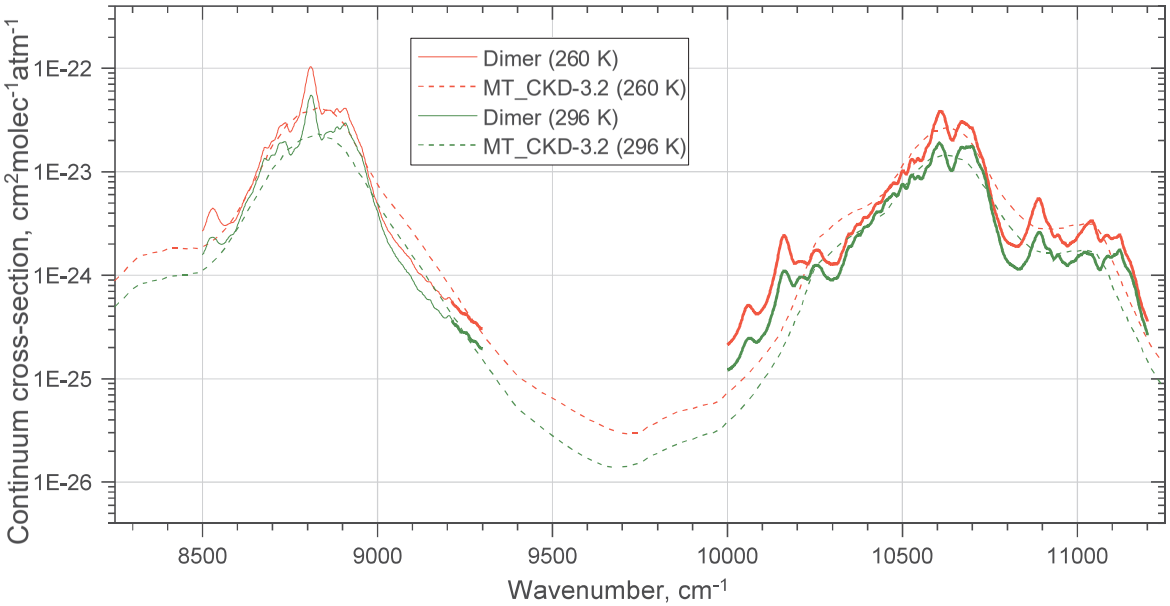

Figure 11

Click here to access/download;Figure;Fig.11.png